HHS Public Access

Author manuscript

Mol Cell. Author manuscript; available in PMC 2020 March 21.

Published in final edited form as:

Mol Cell. 2019 March 21; 73(6): 1267–1281.e7. doi:10.1016/j.molcel.2018.12.010.

BRCA1 haploinsufficiency is masked by RNF168-mediated chromatin ubiquitylation

Dali Zong[1], **Salomé Adam**[2,†], **Yifan Wang**[3,†], **Hiroyuki Sasanuma**[4,†], **Elsa Callén**[1], **Matilde Murga**[5], **Amanda Day**[1], **Michael J. Kruhlak**[6], **Nancy Wong**[1], **Meagan Munro**[2], **Arnab Ray Chaudhuri**[1,7], **Baktiar Karim**[8], **Bing Xia**[9], **Shunichi Takeda**[4], **Neil Johnson**[3], **Daniel Durocher**[2,10], and **André Nussenzweig**[1,11,*]

[1]Laboratory of Genome Integrity, National Cancer Institute, NIH, Bethesda, MD, USA. [2]The Lunenfeld-Tanenbaum Research Institute, Mount Sinai Hospital, Toronto, Ontario, Canada. [3]Molecular Therapeutics Program, Fox Chase Cancer Center, Philadelphia, PA, USA. [4]Department of Radiation Genetics, Graduate School of Medicine, Kyoto University, Kyoto, Japan. [5]Genomic Instability Group, Spanish National Cancer Research Center, CNIO, Madrid, Spain. [6]Laboratory of Cancer Biology and Genetics, National Cancer Institute, NIH, Bethesda, MD, USA. [7]Department of Molecular Genetics, Erasmus University Medical Center, Rotterdam, The Netherlands. [8]Pathology/Histotechnology Laboratory, Frederick National Laboratory for Cancer Research, Frederick, MD, USA. [9]Radiation Oncology, Rutgers Cancer Institute of New Jersey, New Brunswick, NJ, USA. [10]Department of Molecular Genetics, University of Toronto, Toronto, Ontario, Canada. [11]Lead contact

SUMMARY

BRCA1 functions at two distinct steps during homologous recombination (HR). Initially, it promotes DNA end resection, and subsequently recruits the PALB2 and BRCA2 mediator complex, which stabilizes RAD51-DNA nucleoprotein filaments. Loss of 53BP1 rescues the HR defect in BRCA1 deficient cells by increasing resection, suggesting that BRCA1's downstream role in RAD51 loading is dispensable when 53BP1 is absent. Here, we show that the E3 ubiquitin ligase RNF168, in addition to its canonical role in inhibiting end resection, acts in a redundant manner with BRCA1 to load PALB2 onto damaged DNA. Loss of RNF168 negates the synthetic rescue of *BRCA1* deficiency by *53BP1* deletion and predisposes *BRCA1* heterozygous mice to cancer. $BRCA1^{+/-}RNF168^{-/-}$ cells lack RAD51 foci and are hypersensitive to PARP inhibitor, while forced targeting of PALB2 to DNA breaks in mutant cells circumvents *BRCA1*

*Correspondence: andre_nussenzweig@nih.gov.

Author Contributions: D.Z., S.A., Y.W., H.S., E.C., M.M., A.D., M.J.K., N.W., M.M., A. C., B.K. designed and performed experiments; X.B., S.T., N.J., D.D., and A.N. supervised and provided advice. D.Z. and A.N. wrote the manuscript with comments from the authors.

†These authors contributed equally

Declaration of Interests: The authors declare no competing interests

haploinsufficiency. Inhibiting the chromatin ubiquitin pathway may therefore be a synthetic lethality strategy for *BRCA1*-deficient cancers.

Etoc blurb:

BRCA1 facilitates DNA end resection and RAD51 filament formation during homologous recombination. Zong et al. demonstrate that the RNF168-mediated chromatin ubiquitylation pathway acts redundantly with BRCA1 to promote RAD51-dependent homologous recombination. RNF168 activity is essential to prevent overt genome instability and tumorigenesis in *BRCA1* heterozygous mice, independently of *p53* mutation.

Graphical Abstract

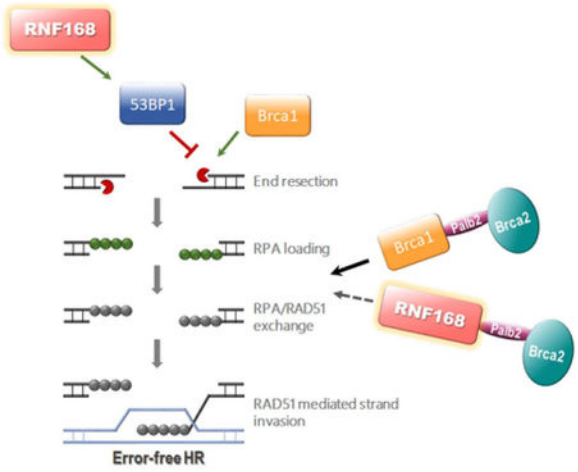

Keywords

Chromatin ubiquitylation; Homologous recombination; Cancer; RNF168; BRCA1; PALB2; RAD51; Haploinsufficiency; Genome stability; Resection; Replication fork protection

INTRODUCTION

BRCA1 and *BRCA2* are caretaker tumor suppressors that maintain genome stability by promoting HR (Kinzler and Vogelstein, 1997). Inheritance of a single mutant allele of *BRCA1* or *BRCA2* significantly increases a person's lifetime risk for developing breast ovarian, prostate and other cancers (Li and Greenberg, 2012; Tutt and Ashworth, 2002). While the tumor suppressor functions of *BRCA1* and *BRCA2* are thought to be haploinsufficient, mouse and cell line-based models of *BRCA1/2* heterozygosity do not display any measurable defects in HR (Sedic and Kuperwasser, 2016). This apparent discrepancy points to the possibility that redundancy in HR could mask latent defects in *BRCA1/2* heterozygous cells. In addition, the mechanisms for haploinsufficiency and carcinogenesis may differ between *BRCA1* and *BRCA2* heterozygous carriers. Supporting this notion, a recent study found that endogenous and environmental toxins induce haploinsufficiency in *BRCA2* mutation carriers by causing the selective proteasomal degradation of BRCA2 without affecting the level of BRCA1 protein (Tan et al., 2017). In

contrast, *BRCA1* deficient cells, but not *BRCA2*-deficient cells, are uniquely sensitive to proteasome inhibitors (Gu et al., 2014).

BRCA1 plays dual roles in HR both by potentiating DNA end-resection and by subsequently delivering RAD51 onto 3' single stranded DNA (ssDNA) substrates. Although its function in end-resection remain unclear, BRCA1 may act in part by removing the end-blocking factor 53BP1 from chromatin surrounding DNA double strand breaks (DSBs), which enables access and long-range resection by the DNA end-processing machinery (Bouwman et al., 2010; Bunting et al., 2010; Callen et al., 2013; Di Virgilio et al., 2013; Escribano-Diaz et al., 2013; Feng et al., 2013; Polato et al., 2014; Zimmermann et al., 2013). In addition, BRCA1 interacts with PALB2 through its coiled-coiled domain, bridging it with BRCA2 post-resection, which in turn, promotes assembly of RAD51 onto 3' ssDNA (Prakash et al., 2015). Since inactivation of *53BP1* stimulates end resection and HR proficiency in *BRCA1*- but not in *BRCA2*- deficient cells, it has been assumed that loss of *53BP1* bypasses the downstream role of BRCA1 in loading RAD51. However, whereas genomic instability and embryonic lethality is rescued in *BRCA1*deficient mouse cells (Bouwman et al., 2010; Bunting et al., 2010; Cao et al., 2009), deletion of *53BP1* exacerbates genome instability in *PALB2* knockout cells (Bowman-Colin et al., 2013), suggesting that *BRCA1*-deficient cells are capable of initiating an alternative mode of RAD51 loading when end-resection is restored.

Here we demonstrate that the RNF168-mediated chromatin ubiquitylation pathway acts redundantly with BRCA1 to promote PALB2- and RAD51-dependent HR. Moreover, RNF168 activity is essential to prevent overt genome instability and tumorigenesis in *BRCA1* heterozygous mice, independently of *p53* mutation. We suggest that the unmasking of *BRCA1* haploinsufficiency by RNF168 deregulation may contribute to tissue-specific cancer predisposition in *BRCA1* mutations carriers.

RESULTS

Chromatin ubiquitylation is essential for HR when BRCA1 is inactivated

The chromatin ubiquitylation pathway consisting of histone H2AX, MDC1, RNF8 and RNF168 regulates the retention of numerous DNA damage response (DDR) proteins including 53BP1 and BRCA1 within a large domain flanking the actual DSB site (Figure 1A) (Altmeyer and Lukas, 2013; Messick and Greenberg, 2009; Pilch et al., 2003). In addition to its established role in promoting NHEJ, the chromatin DDR has been implicated in HR (Adamson et al., 2012; Luijsterburg et al., 2017; Xie et al., 2007; Xie et al., 2004; Zhang et al., 2012). However, the physiological relevance of chromatin ubiquitylation in HR remains unknown. To address this question, we generated a new mouse model for *RNF168* deficiency by gene-targeting (Figures S1A and S1B). Like *53BP1*-deficiency (Bunting et al., 2010; Manis et al., 2004; Ward et al., 2004), *RNF168* ablation led to decreased immunoglobulin class switching (Bohgaki et al., 2011) and increased ssDNA as measured by RPA foci and phosphorylation (Figures S1C-S1E), which were associated with defective 53BP1 foci formation (Figures S1F and S1G). In contrast to *53BP1*$^{-/-}$ cells (Bunting et al., 2010; Bunting and Nussenzweig, 2013), *RNF168*-deficient cells formed aberrant radial chromosomes when treated with PARPi or cisplatin (Figure S1H), and exhibited a mild

reduction in RAD51 foci formation (Figure S1I). Nevertheless, chromatin ubiquitylation appears to be largely dispensable for HR in cells with unperturbed BRCA1 function.

To further determine the relationship between chromatin- and BRCA1-dependent repair, we crossed mice deficient in one allele of full-length BRCA1 (*BRCA1*$^{+/\Delta 11}$) with mice lacking the chromatin DDR genes *H2AX*, *RNF8*, *RNF168* or *53BP1* (Figure 1B). As expected, homozygous *BRCA1*$^{\Delta 11/\Delta 11}$ deletion resulted in embryonic lethality, which was rescued by deleting *53BP1* (Figure 1C) (Bouwman et al., 2010; Bunting et al., 2010; Cao et al., 2009). By contrast, loss of either *H2AX*, *RNF8* or *RNF168* were incompatible with viability when combined with homozygous *BRCA1*$^{\Delta 11/\Delta 11}$ mutation (Figures 1D, S2A and S2B). Moreover, loss of *RNF168* in *BRCA1*$^{\Delta 11/\Delta 11}$*53BP1*$^{-/-}$ mice was lethal (Figure 1E). Thus, unlike 53BP1 deficiency, abrogation of the H2AX-RNF8-RNF168 pathway does not promote BRCA1-independent survival.

Loss of *53BP*1 restored genome stability in *BRCA1*$^{\Delta 11/\Delta 11}$ cells and largely abolished radial chromosome formation (Figure S2C) (Bouwman et al., 2010; Bunting et al., 2010). In contrast, deleting *RNF168* in conditional *BRCA1*$^{F\Delta 11F/\Delta 11}$-mutant B cells (i.e. CD19 CRE *BRCA1*$^{F\Delta 11/F\Delta 11}$*RNF168*$^{-/-}$ mice) exacerbated genome instability to levels well above those produced by each single mutant alone (Figure 1F). Moreover, RAD51 foci formation was severely compromised in the double mutant cells (Figure 1G). Similar synergistic increases in genome instability were observed when either *H2AX* or *RNF8* was deleted in combination with *BRCA1* deficiency (Figure S2D and S2E). Altogether, these results suggest that the H2AX/RNF8/RNF168 chromatin ubiquitylation pathway becomes essential for HR when BRCA1 is functionally inactivated.

RNF168 supports BRCA1-independent HR in human cells

Despite our evidence supporting a crucial role for RNF168 in promoting BRCA1-independent HR in mice, conflicting observations have been made in human cells. Thus, siRNA depletion of RNF168 was reported to suppress the HR defect caused by BRCA1 silencing in human cells (Munoz et al., 2012), while cells co-depleted of BRCA1, 53BP1 and RNF8 showed a reduction in RAD51 foci formation (Nakada et al., 2012). To definitively compare the impact of RNF168 *vs.* 53BP1 loss in human cells lacking BRCA1 and avoid potential confounding factors arising from hypomorphic *BRCA1* alleles, we took advantage of an auxin-based degron system in which BRCA1 protein can be rapidly and conditionally depleted in human TK6 cells (Figures 2A and S3) (Sasanuma et al., 2018). Acute depletion of human BRCA1 resulted in a rapid cessation of proliferation followed by cell death, which was accompanied by a loss of capacity to form RAD51 foci (Figures 2B–2D). In accord with mouse studies (Bouwman et al., 2010; Bunting et al., 2010), deletion of *53BP1* by CRISPR/Cas9 rescued these phenotypes (Figures 2B and 2D). In contrast, deletion of *RNF168* failed to restore the growth defect in BRCA1-depleted cells (Figure 2B). Moreover, RNF168 deficiency did not rescue RAD51 foci formation in BRCA1depleted human TK6 cells (Figures 2C and 2D). Consistent with the observation in TK6, guide RNAs (sgRNA) targeting *RNF168* was able to reverse the PARPi resistant phenotype of human RPE1 cells in which both *BRCA1* and *53BP1* had been deleted using CRISPR-Cas9 (Figures 2E and 2F). Finally, loss of RNF168 significantly impaired damage-

induced RAD51 foci formation in *BRCA1*$^{-/-}$*53BP1*$^{-/-}$ RPE1 cells (Figures 2G–2I). Thus, RNF168 is required to support BRCA1independent survival and RAD51 foci formation in both mouse and human cells.

RNF168 deletion reveals BRCA1 haploinsufficiency

While mutation of a single *BRCA1* allele leads to cancer predisposition, mouse models of *BRCA1* heterozygosity do not show genome instability or tumorigenesis (Berton et al., 2003; Sedic and Kuperwasser, 2016; Xu et al., 2001). Given the severe impact of RNF168 loss in *BRCA1* $^{\Delta 11/\Delta 11}$ cells (Figures 1F and 1G), we wished to determine whether RNF168 activity might also be essential in *BRCA1* heterozygous cells. We first verified that cells derived from *BRCA1*$^{+/\Delta 11}$ and *BRCA1*$^{+/F\Delta 11}$ heterozygous mice express full-length BRCA1 at approximately 50% the level detected in WT controls (Figure 3A). As expected, *BRCA1*$^{+/\Delta 11}$ heterozygous mice expressing RNF168 were born at normal frequency and did not exhibit any notable phenotypes. However, deletion of *RNF168* had a profound impact on the viability of heterozygous *BRCA1*$^{+/\Delta 11}$ mice. Live *BRCA1*$^{+/\Delta 11}$*RNF168*$^{-/-}$ pups were born at significantly sub-Mendelian frequencies, even though both *BRCA1*$^{+/\Delta 11}$ and *RNF168*$^{-/-}$ mice were born at normal frequencies (Figure 3B). While *BRCA1*$^{+/\Delta 11}$*RNF168*$^{-/-}$ embryos were observed on day E16.5 (Figure S4A and S4B), these embryos showed severe growth retardation and stained positive for senescence associated β-galactosidase indicative of senescence (Figures 3C, 3D, S4C and S4D). Moreover, a substantial fraction of *BRCA1*$^{+/\Delta 11}$*RNF168*$^{-/-}$ embryos exhibited additional gross developmental abnormalities, including exencephaly, microphthalmia and anophthalmia (Figures 3C, S4C and S4D). We conclude that *RNF168* loss reveals latent defects associated with *BRCA1* heterozygosity.

Despite the fact that *BRCA1*$^{+/\Delta 11}$*RNF168*$^{-/-}$ pups were born at sub-Mendelian frequencies, we eventually obtained a cohort of live pups through extensive breeding (19 out of 68 expected, total n=727, $p<0.0001$) but they were consistently smaller than their *BRCA1*$^{+/\Delta 11}$ littermates (Figure S4E). *BRCA1*$^{+/\Delta 11}$*RNF168*$^{-/-}$ mice exhibited significantly shortened lifespan with a median survival of 120 days, as compared to either *BRCA1*$^{+/\Delta 11}$ or *RNF168*$^{-/-}$ single mutant littermates (343 and 372 days, respectively) (Figure 3E). Moreover, 9 out of 19 *BRCA1*$^{+/\Delta 11}$*RNF168*$^{-/-}$ mice spontaneously developed lymphoma (Figure S4F), and loss of RNF168 also accelerated tumorigenesis in both *BRCA1*$^{+/\Delta 11}$*p53*$^{-/-}$ and *BRCA1*$^{+/\Delta 11}$*p53*$^{+/-}$ mice (Figures 3F and 3G). Thus, while *p53* deficiency alone does not foster *BRCA1* haploinsufficiency for tumor formation (Berton et al., 2003; Sedic and Kuperwasser, 2016; Xu et al., 2001), *BRCA1* heterozygous mice become tumor prone when RNF168 is lost.

Loss of BRCA1 causes rapid onset of senescence in cultured cells (Cao et al., 2009). Similarly, we found that primary mouse embryonic fibroblasts (MEFs) derived from E13.5 *BRCA1*$^{+/\Delta 11}$*RNF168*$^{-/-}$ embryos grew poorly and senesced prematurely (Figure 3H). By contrast, heterozygous *BRCA1*$^{+/\Delta 11}$ cells grew normally in culture while *RNF168*$^{-/-}$ cells exhibited a relatively mild growth delay (Figure 3H). Moreover, *BRCA1*$^{+/\Delta 11}$*RNF168*$^{-/-}$ MEFs and splenic B cells exhibited high levels of genome instability when exposed to PARPi or cisplatin (Figures 3I, S5A and S5B), in a manner dependent on H2A-K13/K15

ubiquitylation, as inferred using the separation-of-function RNF168^{R57D} mutant (Mattiroli et al., 2012) (Figure 3J). Finally, *BRCA1*$^{+/\Delta 11}$*RNF168*$^{-/-}$ cells exhibited reduced short-term viability and clonogenic survival upon treatment with PARPi and cisplatin (Figures S5C-S5F). Together, these data demonstrate that BRCA1 becomes haploinsufficient for genome maintenance in the absence of H2A-directed RNF168 ubiquitin ligase activity.

BRCA1 independent PALB2 loading requires RNF168

It was recently demonstrated that RNF168 promotes an alternative mode of recruitment of PALB2 to damaged chromatin (Luijsterburg et al., 2017). Since RNF168 is dispensable for RAD51 foci (Figure S1I) and organismal viability whereas PALB2 is essential (Bowman-Colin et al., 2013; Rantakari et al., 2010), absence of the chromatin ubiquitin pathway alone should not abrogate HR *in vivo*. In agreement with Luijsterburg et al., we found that the H2A ubiquitylation activity of RNF168, but not 53BP1, promoted the formation of irradiation-induced PALB2 foci (Figures S6A and S6B). Since BRCA1 is a major facilitator of PALB2 recruitment (Sy et al., 2009; Zhang et al., 2009a; Zhang et al., 2009b), we hypothesized that RNF168 deficient cells might still be able to recruit PALB2 to DNA damaged sites, insufficient to be observed as distinct foci, but ample enough to load RAD51.

To examine DSB recruitment independent of large-scale focal accumulation (BekkerJensen et al., 2006; Celeste et al., 2003), we subjected cells to laser micro-irradiation and measured the accumulation of PALB2 along the damaged tracks marked by γ-H2AX. Compared to WT cells, *BRCA1*$^{+/\Delta 11}$ cells and *RNF168*$^{-/-}$ cells exhibited a reduction in PALB2 accumulation at damage sites, but PALB2 recruitment was barely detectable in *BRCA1*$^{+/\Delta 11}$*RNF168*$^{-/-}$ cells (Fig. 4A). Moreover, while *RNF168*$^{-/-}$ and *BRCA1*$^{+/\Delta 11}$ cells were largely competent for RAD51 foci formation (Figures S1I and S6C), there was a severe defect in RAD51 loading in *BRCA1*$^{+/\Delta 11}$*RNF168*$^{-/-}$ cells (Figure 4B), which correlated with the synergistic increase in genome instability (Figures 3I, S5A and S5B). Thus, BRCA1 and RNF168 act cooperatively to facilitate RAD51 assembly and maintain genome stability.

In contrast to the severe impact of RNF168 loss in *BRCA1*-deficient cells, loss of RNF168 in *BRCA2*-deficient cells did not further enhance genome instability (Figure S6D). These data suggest that BRCA1-independent RAD51 loading via PALB2/BRCA2 requires RNF168. Consistent with this, inactivation of *PALB2* or *BRCA2* by CRISPR-Cas9 re-sensitized *BRCA1*$^{-/-}$*53BP1*$^{-/-}$ human RPE1 cells to PARPi (Figure S6E), similar to *RNF168* deletion (Figure 2F). Thus, *BRCA1* heterozygous cells and *BRCA1*$^{-/-}$*53BP1*$^{-/-}$ cells rely on RNF168 to sustain a critical level of PALB2 recruitment that is sufficient for RAD51-dependent HR and normal growth.

To determine whether RNF168-mediated PALB2 recruitment is separable from the canonical BRCA1-dependent PALB2 response, we took advantage of a recent mouse model in which mutations have been introduced into the PALB2 coiled-coil domain to produce a mutant PALB2 protein (PALB2^{CC6}) that is unable to interact with BRCA1 (Figure 4C) (Simhadri et al., 2014). Unlike mice with a complete knockout of *PALB2* or *BRCA1*, *PALB2*$^{CC6/CC6}$ mice are viable, suggesting another loading platform for PALB2 could substitute for BRCA1 (Simhadri et al., 2014). Similar to *BRCA1/RNF168*-deficiency,

combining *PALB2*$^{CC6/CC6}$ homozygosity with *RNF168* deficiency was incompatible with viability and *PALB2*$^{CC6/CC6}$*RNF168*$^{-/-}$ embryos died before E16.5 (Figures 4D and S6F). Moreover, partial loss of the PALB2/BRCA1 interaction in *PALB2*$^{+/CC6}$ *RNF168*$^{-/-}$ cells led to increased PARPi- and cisplatin-induced genomic instability relative to *PALB2*$^{+/CC6}$, *RNF168*$^{-/-}$ or even *PALB2*$^{CC6/CC6}$ cells (Figure S6G and S6H). Thus, when either BRCA1 levels or its interaction with PALB2 is decreased by 50%, cells rely on the RNF168-dependent mode of PALB2 recruitment to sustain HR.

Forced loading of PALB2 to chromatin bypasses BRCA1 haploinsufficiency

Based on the observation that RNF168 ubiquitin ligase activity is critical for genome integrity in *BRCA1*$^{+/\Delta 11}$ cells, we hypothesized that the requirement for RNF168 activity in *BRCA1*$^{+/\Delta 11}$ cells might be circumvented if PALB2 could be forced to accumulate at DNA breaks. To accomplish this, we fused the FHA domain of RNF8, which recognizes phosphorylated MDC1 at sites of DNA damage (Huen et al., 2007; Kolas et al., 2007; Mailand et al., 2007), in frame to PALB2 (Figure 4E). The resultant fusion protein, PALB2^{FHA}, was able to form foci in response to DNA damage in cells lacking RNF168 (Figures 4F and 4G). PALB2^{FHA} also restored RAD51 foci formation in *BRCA1*$^{+/\Delta 11}$*RNF168*$^{-/-}$ cells to levels comparable to those found in WT controls (Figures 4F and 4G). Moreover, PALB2^{FHA} expression reduced the formation of toxic chromosomal radials in *BRCA1*$^{+/\Delta 11}$*RNF168*$^{-/-}$ cells (Figure 4H) and alleviated their hypersensitivity to PARPi (Figure 4I). Thus, the requirement of RNF168 for genome maintenance in *BRCA1* heterozygous cells can be bypassed by augmenting PALB2 binding to damaged chromatin.

Chromatin ubiquitylation is dispensable in BRCA1 mutants that retain interaction with PALB2

The risk of carcinogenesis among mutation carriers is dependent on the nature of the germline *BRCA1* mutation (Wang et al., 2016a). A mutant form of BRCA1 lacking exon 11 (BRCA1Δ11q) was found to be expressed in human breast cancer cells and showed reduced efficiency of interaction with PALB2 compared to full-length BRCA1 (Wang et al., 2016a) (Figure 5A). As BRCA1-Δ11q is nearly identical to the mouse BRCA1-Δ11 protein, we hypothesize that this explains why mutant *BRCA1*$^{+/\Delta 11}$, *BRCA1*$^{\Delta 11/\Delta 11}$ and *BRCA1*$^{\Delta 11/\Delta 11}$*53BP1*$^{-/-}$ cells become reliant on RNF168 for loading RAD51. Indeed, even *BRCA1*$^{+/\Delta 11}$ cells showed a reduction in PALB2 accumulation at damage sites (Figure 4A). By contrast, a mutant form of BRCA1 lacking the N-terminal RING domain (BRCA1-ΔRING) (Drost et al., 2016; Wang et al., 2016b) was able to maintain interaction with PALB2, BRCA2 and RAD51 similar to full-length BRCA1 (Figure 5A).

Mice carrying homozygous deletion of *BRCA1* exon 2 produce a mutant RING-less BRCA1 protein (BRCA1-Δ2) that is structurally similar to human BRCA1-ΔRING (Li et al., 2016). Since BRCA1-Δ2 maintains an intact PALB2 interaction domain (Drost et al., 2016; Li et al., 2016; Wang et al., 2016b), we speculated that *BRCA1*$^{\Delta 2/\Delta 2}$ mice would not be reliant on RNF168-dependent pathway for loading PALB2 (Figure 5B). Consistent with this, and contrary to the synthetic lethality imparted on *BRCA1*$^{\Delta 11/\Delta 11}$ *and BRCA1*$^{+/\Delta 11}$ mice, RNF168 deficiency rescued the early embryonic lethality in *BRCA1*$^{\Delta 2/\Delta 2}$ mice (Ludwig et al., 1997) (Figure 5C). *BRCA1*$^{\Delta 2/\Delta 2}$ *RNF168*$^{-/-}$ mice survived at least 143 days (median

survival 275 days), similar to mice lacking only *RNF168* (median survival 281 days), and were not more tumor prone than the latter (Figure 5D). On the contrary, *BRCA1*$^{+/\Delta 11}$ *RNF168*$^{-/-}$ mice had shorter median survival (120 days) and developed tumors at a younger age (Figure 3E and Figure S4F). *BRCA1*$^{\Delta 2/\Delta 2}$ *RNF168*$^{-/-}$ cells exhibited only slightly higher levels of PARPi-induced radial chromosomes to those observed in *RNF168*$^{-/-}$ cells (Figure 5E). Moreover, while RAD51 foci formation was severely compromised in conditionally deleted *BRCA1*$^{F\Delta 2/F\Delta 2}$ MEFs (marked by loss of BARD1 protein), RAD51 foci were largely restored in *BRCA1*$^{\Delta 2/\Delta 2}$ *RNF168*$^{-/-}$ MEFs derived from compound homozygous mutant mice (Figures 5F and 5G). These data are consistent with the idea that increased resection alone can circumvent the HR defects in *BRCA1* mutants that maintain their interaction with PALB2. However, rescuing *BRCA1* mutants with impaired BRCA1/PALB2 interaction requires both increased resection and RNF168-dependent PALB2 loading.

RNF168 does not cooperate with BRCA1 in replication fork protection

Recent studies suggest that replication stress response pathways may be partially defective in cells from heterozygous *BRCA1* and *PALB2* mutation carriers (Nikkila et al., 2013; Pathania et al., 2014). Moreover, the inability to protect stalled replication forks contributes to DNA damage-induced cytotoxicity (Ray Chaudhuri et al., 2016). This raises the possibility that PARPi and cisplatin hypersensitivity evident in *BRCA1*$^{+/\Delta 11}$*RNF168*$^{-/-}$ cells could result from defects in replication fork protection as well as HR. However, loss of *RNF168* did not further increase nucleolytic degradation of replication forks regardless of *BRCA1* mutation (*BRCA1*$^{+/\Delta 11}$ or *BRCA1* $^{\Delta 2/\Delta 2}$) (Figures 6A and 6B). Interestingly, the BRCA1 RING domain, though essential for HR, was dispensable for replication fork protection, whereas *BRCA1* exon 11 is essential for both (Ray Chaudhuri et al., 2016). We conclude that impairment of RAD51-dependent HR, but not replication fork protection, underlies the synthetic lethal interaction between *BRCA1*$^{+/\Delta 11}$ and *RNF168*.

DISCUSSION

The γ-H2AX/RNF8/RNF168 ubiquitin cascade triggers DNA repair factor recruitment to chromatin flanking DSBs through sequential ubiquitylation of histones H1 and H2A (Doil et al., 2009; Stewart et al., 2009; Stucki et al., 2005; Thorslund et al., 2015; Wilson et al., 2016). Chromatin ubiquitylation is required for the concentration and spreading of DNA damage response proteins distal to the actual break site but is dispensable for proximal break-site recruitment (Bekker-Jensen et al., 2006; Celeste et al., 2003). The precise function of chromatin ubiquitylation surrounding break sites remains unclear, as deficiency in H2AX/RNF8/RNF168 impairs a subset of chromatin-related DSB repair/signaling functions, none of which are essential for viability (Bohgaki et al., 2011; Celeste et al., 2002; Santos et al., 2010).

Our results indicate that in addition to opposing the initial resection step of HR, the ubiquitin pathway acts as a backup to BRCA1 at a later step of HR that connects it with PALB2 and RAD51 (Figure 6C). Similar to BRCA1 (Bekker-Jensen et al., 2006; Coleman and Greenberg, 2011; Hu et al., 2011; Messick and Greenberg, 2009), PALB2 appears to engage

both the flanking chromatin and the ssDNA compartments proximal to DSBs. While BRCA1directed PALB2 recruitment to ssDNA is critical for RAD51 dependent HR (Sy et al., 2009; Zhang et al., 2009a; Zhang et al., 2009b), the physiological relevance of RNF168-mediated PALB2 chromatin loading remained unclear (Luijsterburg et al., 2017). Based on our finding that cells become reliant on the RNF168-dependent pathway when BRCA1 protein level or its interaction with PALB2 is reduced by 50%, we suggest that ubiquitin polymers on histones assembled on ssDNA after end resection (Adkins et al., 2017; Huang et al., 2018) or surrounding the processed ssDNA compartment, provide a backup mechanism to load RAD51 (Figure 6C). In *BRCA1/53BP1*-deficient cells, such a ubiquitin platform becomes essential to restore HR and viability. In contrast, the spread of chromatin ubiquitin conjugates around DSBs is dispensable in BRCA1 mutants that retain efficient binding to PALB2. In this case, increased resection alone is sufficient to restore HR.

Targeting chromatin ubiquitylation promotes synthetic lethality

When HR is rewired in such a way that it becomes reliant on the chromatin ubiquitin pathway, this leads to vulnerabilities that may be targeted to induce synthetic lethality. For example, it was shown that inhibition of ATR profoundly sensitizes PARPi-resistant *BRCA1*-deficient cell lines (Yazinski et al., 2017). Similarly, ATM inhibition exacerbates the HR defect in *BRCA1*-deficient cells (Bunting et al., 2010; Chen et al., 2017). One possibility is that in addition to their function in promoting end-resection (Cuadrado et al., 2006; Jazayeri et al., 2006; Peterson et al., 2013; Shiotani and Zou, 2009), ATM/ATR-mediated signaling of H2AX emanating from the DSB site supports RNF168 recruitment and activity, which in turn cooperates with BRCA1 to load RAD51. Consistent with this idea, it was shown that in *BRCA1*-deficient cells, ATR becomes essential for BRCA2 localization (Yazinski et al., 2017). Therefore, targeting the DSB-induced chromatin ubiquitylation pathway may provide a unique therapeutic opportunity for treatment of *BRCA1*-deficient cancers that become resistant to PARPi. In addition to PARPi, proteasome inhibitors have been reported as selective *BRCA1*-targeting agents (Gu et al., 2014). Proteasome inhibitors profoundly impair the accumulation of RNF168 but not γ-H2AX, MDC1 or RNF8 at DNA damage sites (Doil et al., 2009; Stewart et al., 2009). Our data are therefore consistent with the idea that proteasome inhibition is synthetic lethal with *BRCA1*-deficiency because of the redundancy between RNF168 and BRCA1 in HR.

Deregulation of chromatin ubiquitylation can promote BRCA1 haploinsufficiency

What triggers cancer in humans with heterozygous *BRCA1* mutations remains unclear. While *BRCA1* heterozygosity supports HR, recent evidence indicates that mammary epithelial cells with one germline mutated *BRCA1* allele exhibit genome instability and increased replication stress (Pathania et al., 2014; Sedic and Kuperwasser, 2016). Our data suggest that *BRCA1* haploinsufficiency is masked by RNF168, and latent HR defects are only revealed when RNF168 levels or activity becomes lower than a certain threshold. Recent studies reveal that RNF168 protein stability is limited by the ubiquitin E3 ligases TRIP12 and UBR5 (Gudjonsson et al., 2012). Moreover, RNF168-mediated ubiquitylation signaling becomes saturated when the number of DNA breaks exceeds approximately twenty (Gudjonsson et al., 2012). Thus, if RNF168 activity is low in a few select tissues, either because of deregulated expression of RNF168 suppressors, or because excessive replication

stress leads to spontaneous DSBs in *BRCA1* heterozygotes (Pathania et al., 2014), the resultant insufficient spreading of chromatin modifications would trigger a defect in HR, leading to genomic instability. In this way, deregulation of the chromatin ubiquitylation pathway could result in tissue-specific predisposition to cancer development in *BRCA1* mutant carriers.

STAR METHODS

METHOD DETAILS

Mice—The embryonic stem cell line JM8A3.N1.C2 was used to generate RNF168 deficient mice at the Transgenic Mouse Model Laboratory (Frederick National Laboratory for Cancer Research). Three derivative clones (HEPD0798_7_D9, HEPD0798_7_B10, HEPD0798_7_F12) (Toronto Centre for Phenogenomics), in which the *RNF168* gene was disrupted by insertion of a neomycin gene selection cassette into exon 2, were injected into C57BL/6 blastocysts. The resultant chimeric offspring were backcrossed with wildtype C57BL/6 mice, producing $RNF168^{+/-}$ animals. Germline transmission of the targeted allele was confirmed by PCR (forward, 5'-TGACATTCCACACCACTTTCTAGC; reverse, 5'-CAACGGGTTCTTCTGTTAGTCC) in DNA extracted from tail clips and an alternate (5'-CAAGGAAACAAACAGCGTTAGGGC) reverse primer was used to amplify the non-targeted wildtype allele. Finally, heterozygotes were further intercrossed to generate homozygous $RNF168^{-/-}$ mice.

$BRCA1^{+/\Delta 11}$ (germline), $BRCA1^{F\Delta 11/F\Delta 11;\ CD19Cre}$, $BRCA2^{F/F;\ CD19Cre}$ (conditional) mice were obtained from the NCI mouse repository. $P53^{+/-}$ mice were obtained from Taconic Biosciences. $BRCA1^{\Delta 11/F\Delta 11;\ CD19Cre}$ mice were generated by crossing $BRCA1^{F\Delta 11/F\Delta 11;\ CD19Cre}$ mice with $BRCA1^{+/\Delta 11}$ mice. Germline $BRCA1^{+/\Delta 2}$ and conditional $BRCA1^{F\Delta 2/F\Delta 2;\ CD19Cre}$ mice were kindly provided by Dr. Thomas Ludgwid. $53BP1^{-/-}$, $H2AX^{-/-}$, $RNF8^{-/-}$, $PALB2^{CC6/CC6}$ mice have been described (Celeste et al., 2002; Santos et al., 2010; Simhadri et al., 2014; Ward et al., 2003). All breeding and experimentation involving mice followed protocols approved by the National Institutes of Health Institutional Animal Care and Use Committee.

Senescence-associated β-galactosidase staining—Mouse embryos were extracted on day E16.5 following timed pregnancies and fixed in 2% formaldehyde and 0.2% glutaraldehyde for 45 min. After thorough washing in PBS, the fixed embryos were stained for senescence associated β-galactosidase activity using a commercially available kit (Cell Signaling Technology), as per manufacturer's instructions.

Cell culture

Mouse embryonic fibroblasts: To isolate primary mouse embryonic fibroblasts (MEFs), E13.5 embryos were first minced with scissors and then trypsinized. The liberated cells were incubated in Dulbecco's Modified Eagle's Medium (DMEM, Gibco) supplemented with 15% heat-inactivated fetal bovine serum (FBS, Gemini Bio-Products) and 1% penicillin + streptomycin (Gibco). For growth assays, 100,000 primary MEFs from passages 3–4 are

plated in triplicate 60 mm dishes. Cell numbers were recorded on consecutive days for seven (*WT*, *RNF168*$^{-/-}$, *BRCA1*$^{+/\Delta 11}$) or fourteen days (*BRCA1*$^{\Delta 11/\Delta 11}$, *BRCA1*$^{+/\Delta 11}$*RNF168*$^{-/-}$).

To establish immortalized MEF cell lines, primary MEFs between passages 2–4 were transiently transfected with a vector encoding SV40 T-antigen (pCMV-SV40T). SV40immortalized MEFs were routinely cultured in DMEM supplemented with 10 or 15% FBS.

Mouse B cells—Resting primary B cells were isolated from the spleen using anti-CD43 microbeads (Miltenyi Biotec). Purified cells were resuspended in complete B cell medium containing 25 μg/ml LPS, 5 ng/ml IL-4 (both Sigma-Aldrich) and 0.5 μg/ml anti-CD180 (BD Biosciences) to stimulate proliferation and immunoglobulin class switch recombination (CSR). Successful *ex vivo* CSR was assayed on day 3 by flow cytometry following live cell staining using biotinylated antiIgG1 and FITC conjugated anti-B220 antibodies (BD Biosciences). Analysis of FACS data was done using FlowJo (version 10).

Human cell lines—TK6 cells were grown in RPMI-1640 GlutaMax™ medium supplemented with 10% horse serum (both from Gibco). RPE1 cells were cultured in DMEM supplemented with 10% FBS. All culture medium contained 1% penicillin + streptomycin.

Generation of gene-targeted TK6 cells—To construct targeting vectors for the endogenous *BRCA1* locus (Sasanuma et al., 2018), the left and right homology arms were amplified using the following sets of primers: left arm-F, 5'-AGGGCGAATTGGAGCTCCCCCAGATTGAAGTTCATGTTAATACAG and left arm-R, 5'-TTGGCGCCTGCACCGGATCCGTAGTGGCTGTGGGGGATCTGGGGT; right arm-F, 5'CGAAGTTATTAGGTCCCTCGTAGTCCAGGAGAATGAATTGACACT and right arm-R, 5'GGGAACAAAAGCTGGGGAACCTCTTCTCACTGTCACCCAGGCTGGAGTGC. The guide RNA (gRNA) recognition sequence (5'-GGAGTCGATTGATTAGA) was removed from the left homology arm to prevent unwanted digestion by CRISPR-Cas9. Both homology arms were subsequently assembled into each of two vectors encoding the auxin-inducible degron (AID), pBS-mAID-GFP-loxP-NEO^{R} (digested with EcoNI/SmaI) and pBS-mAID-GFP-loxP-HIS^{R} (digested with EcoNI/BamHI), respectively, using the GeneArt Seamless Cloning Enzyme Mix (Thermo Fisher). The gRNA was inserted into the BbsI site of pX330 (Addgene). The resulting pX330-gRNA vector was co-transfected along with the *BRCA1* targeting vectors into *WT* and *53BP1*$^{-/-}$ TK6 cells expressing the *TIR1* ubiquitin ligase gene (Sasanuma et al., 2018).

To construct targeting vectors for the *RNF168* gene, the left and right homology arms (~1 kb) were amplified using the following sets of primers: left arm-F, 5'-GCGAATTGGGTACCGGGCCGCCTGGATAAAACAGTGAGACCCCA and left arm-R, 5'-CTGGGCTCGAGGGGGGGCCGGCGTCTTTGGGTAGAGCCATTTCA; right arm-L, 5'TGGGAAGCTTGTCGACTTAATCGAAAAGGCGAGTTTATGCTGTC and right arm-R, 5'CACTAGTAGGCGCGCCTTAAGCTTATTGCTCACATTAGTGGAGG. Both homology arms were assembled into each of two ApaI/AflII-digested expression vectors, pDT-ApA/HYGRO^{R} and pDT-ApA/BSR^{R}, respectively, using the GeneArt Seamless Cloning Enzyme

Mix. Two gRNAs targeting *RNF168* (5'-ACTGGCACTCGGACAGCGAG; 5'-GGAGGGTGACGGGCTCCACG) were individually inserted into the BbsI site of pX330. The resulting pX330-gRNA vectors were co-transfected along with the *RNF168* targeting vectors into *BRCA1*$^{AID/AID}$ TK6 cells. After transfection, cells were released into 20 ml drug-free medium containing 10% horse serum. Forty-eight hours after transfection, cells were seeded into 96-well plates and grown in medium containing hygromycin and blasticidin for two weeks. Surviving single cell-derived clones were validated for homozygous gene targeting by PCR using the following primers: HYGRO^{R}_F (5'-ATCTTTGTAGAAACCATCGGCGCAGCTATT)/BSR^{R}_F (5'-GAATTGCCGCTCCCACATGATGTTTATTAT) and RNF168_CHK_R (5'-CACGAGAGAACGGAGACACCATATCCTAAG). Cells were treated with indicated doses of the PARP inhibitor Olaparib (Selleckchem) or cisplatin (Sigma-Aldrich) continuously for 10 days (Olaparib) or for 24 h followed by a 9-day post-incubation in drug-free medium (cisplatin). Thereafter, culture dishes were stained with 0.5% crystal violet and colonies containing >50 cells were tallied.

Cell viability assay—Twenty-four hours post cytokine stimulation, primary activated B cells were treated with either vehicle, 1 μM PARPi or 0.5 μM cisplatin continuously for 48 h. Thereafter, cell viability was determined using the CellTiter-Glo Luminescent Cell Viability Assay (Promega) as per manufacturer's instructions.

Multicolor growth competition assay (MCA)—Generation of hTERT-RPE1 *BRCA1*$^{-/-}$*53BP1*$^{-/-}$*p53*$^{-/-}$ FLAG-Cas9 cells has been described (Noordermeer et al., 2018). One hundred thousand cells were infected at an MOI of ~1.2 to ensure 100% transduction efficiency with either virus particles of NLS-mCherry LacZ-sgRNA or NLS-GFP GOI-sgRNA (RNF168, PALB2, BRCA2 or the empty vector). Ninety-six hours after transduction, mCherry- and GFP-expressing cells were mixed 1:1 (3,000 cells + 3,000 cells) and seeded in 12-well plates. During the course of the experiment, cells were subcultured when near confluency was reached. Cells were imaged for GFP- and mCherry signal the day of initial plating ($t = 0$) and on days 3, 7, 10, 14 and 17 using the automated IN Cell Analyzer (GE Healthcare Life Sciences) with a 4X objective. An Acapella script (PerkinElmer) was used to segment and quantify the number of GFP-positive and mCherry-positive cells. Efficiency of indel formation was determined by PCR amplification of the region surrounding To induce degradation of AID-tagged BRCA1 protein, auxin (3-indoleacetic acid, Sigma-Aldrich) was added to the cell culture medium (500 μM final concentration). For growth assay, cell numbers were recorded for seven consecutive days.

Plasmids, transfection and viral transduction—Retroviral pMX-PIE-based vectors encoding wildtype human RNF168 and the catalytic dead (R57D) mutant have been described (Zong et al., 2015). cDNA corresponding to wildtype human PALB2 was amplified by PCR from pDEST-FRT-TO-GFP-PALB2 (Orthwein et al., 2015), and subcloned into the multiple cloning site of pMX (no IRES-GFP), producing pMX-GFP-PALB2. Retroviral vector encoding PALB2^{FHA} was produced by PCR amplification of the FHA domain of RNF8 from pMX-RNF8(FHA)-RNF168 and subcloned into pMX-GFP-PALB2 between GFP and PALB2. Infection-competent retroviral particles were assembled

in BOSC23 cells co-transfected with the pCL-ECO helper virus. Retroviral supernatant was collected 40–48 h later to transduce MEFs and B cells.

Pre-made adenovirus (Ad5-CMV-GFP and Ad5-CMV-Cre-GFP, Addgene) was used at a MOI of 100 to transduce MEFs.

Mammalian expression vectors encoding GFP-tagged PALB2 (pDEST-FRT-TO-GFP-PALB2), FLAG-tagged PALB2 (pDEST-FRT-TO-FLAG-PALB2) have been described (Orthwein et al., 2015). Transient expression was achieved by transfection in MEFs using the XtremeGENE 9 DNA transfection reagent (Roche Diagnostics), as per manufacturer's instructions.

Colony formation assay—the sgRNA sequence and TIDE analysis on DNA isolated from GFP-expressing cells 6 days post-transduction.

Metaphase spread analysis—Activated cycling B cells and asynchronous MEFs were treated with 1 μM PARPi (24 h) or 0.5 μM cisplatin (18 h) and subsequently arrested at mitosis with colcemid (Invitrogen). Cells were incubated in pre-warmed KCl (Sigma-Aldrich, 75 mM) for 20 minutes in a 37°C water bath to induce swelling and then fixed in methanol/glacial acetic acid (ratio 3:1). Droplets of cells were spread onto glass slides inside a cytogenetic drying chamber (Thermotron). Fluorescence *in situ* hybridization was performed with a Cy3-labeled $(CCCTAA)_3$ peptide nucleic acid probe (PNA Bio) to stain telomeres, and DNA was counterstained with DAPI (Callen et al., 2013). Images were captured with the Metafer automated scanning and imaging platform (MetaSystems). One hundred metaphases were scored for the presence of chromosomal aberrations.

Immunoblotting and immunoprecipitation—For immunoblotting, cells were lysed in a buffer containing 50 mM Tris-HCl (pH 7.5), 200 mM NaCl, 5% Tween-20, 2% Igepal CA-630, 2 mM PMSF, 50 mM β-glycerophosphate (all from Sigma-Aldrich) and protease inhibitor cocktail tablet (cOmplete Mini, Roche Diagnostics). Equal amounts of lysates were loaded into precast mini-gels (Invitrogen) and resolved by SDS-PAGE. Transfer of proteins onto nitrocellulose membranes and incubation with primary/secondary antibodies were performed according to standard procedures. Visualization of protein bands was achieved by either enhanced chemiluminescence (Amersham) or fluorescence imaging (LI-COR Biosciences).

For co-immunoprecipitation experiments, mCherry (mCh), BRCA1-full length (FL), BRCA1-ΔRING (del aa1–127) and BRCA1-Δ11q (del aa264–1366) proteins were ectopically expressed in MD-MBA-436 cells (Wang et al., 2016a; Wang et al., 2016b). Nuclear extracts were prepared using NE-PER Nuclear and Cytoplasmic Extraction Reagents (Thermo Fisher Scientific) according to manufacturer's instructions. HA antibody was then used to pull down tagged BRCA1 complexes from 3 mg of nuclear extract using Pierce Classic IP Kit (Thermo Fisher Scientific). Because ectopic BRCA-Δ11q was expressed at significantly higher levels than BRCA1-FL and BRCA1-ΔRING, different volumes of IP elution were loaded in protein mini-gels in order to achieve similar loading of all three BRCA1 isoforms. Samples were subsequently resolved by standard SDS-PAGE.

BRCA1 binding partners were detected by antibodies recognizing BRCA2, PALB2, and RAD51.

Immunofluorescence and laser microirradiation—For immunofluorescence staining, cells grown on coverslips were first incubated in culture medium containing 10 μM EdU (Invitrogen) for 20 min prior to γ-irradiation (^{137}Cs Mark 1) (JL Shepherd). Thereafter, cells were pre-extracted (20 mM HEPES, 50 mM NaCl, 3 mM $MgCl_2$, 0.3 M sucrose, 0.2% Triton X-100) on ice for 5 min to remove soluble nuclear proteins. Extracted samples were fixed (4% paraformaldehyde), permeabilized (0.5% Triton X-100), incubated with appropriate primary antibodies followed by appropriate fluorochrome-conjugated secondary antibodies (Invitrogen). Next, click-IT chemistry was performed as per manufacturer's instructions and DNA was counterstained with DAPI (Thermo Fisher Scientific). Images were captured at 63X magnification with an AxioCam MRc5 mounted on an Axio Observer Z1 epifluorescence microscope (Zeiss).

For laser microirradiation, cells grown in 35 mm glass bottom microwell dishes (MatTek) were first pre-sensitized in DMEM medium containing 0.1 μg/ml of Hoechst 33342 for 60 min before replacing it with fresh medium containing 10 μM EdU. After incubating for 20 min, the EdU-containing medium was replaced with phenol red free medium (FluoroBrite, Invitrogen) and cells were irradiated with the 364 nm laser line on a LSM510 confocal microscope (Zeiss) equipped with a heated stage. Cells were allowed to recover for 10–15 min prior to pre-extraction (5 min on ice) and processing for immunofluorescence. ZEN Blue (Zeiss) was used to quantify fluorescence intensities of laser stripes.

DNA fiber assay—Asynchronous MEFs or B cells were labelled with 50 μM CldU for 30min, washed with warm PBS and then sequentially to 250 μM IdU for 30min. After completion of IdU labeling, cells were washed again in warm PBS and incubated with 4mM HU for 3 hours before they were collected and resuspended in cold PBS at a concentration of 0.5×10^6/ml. A volume of 2.5 μl of cell suspension was lysed in 7.5 μl of lysis buffer (200 mM Tris-HCl (pH 7.4), 50 mM EDTA, 0.5% SDS) on glass slides for 8min before DNA fibers were stretched. Fibers were then fixed in cold methanol/glacial acetic acid (ratio 3:1) for 2 minutes, air-dried and left overnight at 4 °C. Preparations were rehydrated in PBS and denatured in 2.5 M HCl for 30min, washed with PBS and blocked in PBS containing 2% BSA and 0.2% Tween-20 for 1 hour. Newly replicated DNA tracks were immunostained using anti-BrdU antibodies recognizing CldU (Becton Dickinson, Cat# 347580, 1:100 dilution) and IdU (Abcam, ab6326, 1:100). Secondary antibodies used were goat anti-mouse Alexa Fluor 488 (Molecular Probes, Cat# A11001, 1:200) and anti-rat Cy3 (Jackson ImmunoResearch, Cat# 712-166-153, 1:200). Images were captured at 40X magnification using an Axio Observer Z1 (Zeiss). DNA fiber length was measured using ImageJ software.

Statistics—Statistical significance was calculated using unpaired two-tail *t*-test unless otherwise specified. Chi-square (χ^2) test for goodness of fit was used to compare expected and observed frequencies of live born pups. Mann-Whitney test was used for comparing DNA fiber lengths and PALB2 accumulation along laser-induced stripes. Kaplan-Meier survival analyses (Mantel-Cox test) were used for all survival and tumor studies. All

statistical tests were performed in GraphPadPrism except χ^2 tests, which were done in RStudio.

Supplementary Material

Refer to Web version on PubMed Central for supplementary material.

Acknowledgments:

We thank Sergio Ruiz-Macias, Avinash Bhandoola, Haico van Attikum, Niels Mailand and Nussenzweig lab members for stimulating discussions; Yaakov Maman and Sriram Sridharan for help with statistical analysis; Sam Bunting for *BRCA1*$^{+/\Delta 2}$ mice; Jennifer Wise, Kelly Smith, Raymond Hui and Breana Myers for assistance with animal work. M.M. was funded by a grant from the Salvador Madariaga Program (PRX18/00364) from the Spanish Ministry of Education, Culture and Sports, within the framework of the National Program of Talent Promotion and its usefulness in R&D&I, National Mobility Subprogram, National Plan of R&D&I. The A.N. laboratory is supported by the Intramural Research Program of the NIH, an Ellison Medical Foundation Senior Scholar in Aging Award (AG-SS-2633–11), the Department of Defense Idea Expansion (W81XWH-15-2-006), and Breakthrough (W81XWH-16-1-599) Awards, the Alex Lemonade Stand Foundation Award, and an NIH Intramural FLEX Award. The work was also supported by the Rutgers Cancer Institute and NCI-CCR Partnership on DNA Repair and Genomic Instability in Cancer.

References:

Adamson B, Smogorzewska A, Sigoillot FD, King RW, and Elledge SJ (2012). A genome-wide homologous recombination screen identifies the RNA-binding protein RBMX as a component of the DNA-damage response. Nat Cell Biol 14, 318–328. [PubMed: 22344029]

Adkins NL, Swygert SG, Kaur P, Niu H, Grigoryev SA, Sung P, Wang H, and Peterson CL (2017). Nucleosome-like, Single-stranded DNA (ssDNA)-Histone Octamer Complexes and the Implication for DNA Double Strand Break Repair. J Biol Chem 292, 5271–5281. [PubMed: 28202543]

Altmeyer M, and Lukas J (2013). To spread or not to spread--chromatin modifications in response to DNA damage. Curr Opin Genet Dev 23, 156–165. [PubMed: 23312207]

Bekker-Jensen S, Lukas C, Kitagawa R, Melander F, Kastan MB, Bartek J, and Lukas J (2006). Spatial organization of the mammalian genome surveillance machinery in response to DNA strand breaks. J Cell Biol 173, 195–206. [PubMed: 16618811]

Berton TR, Matsumoto T, Page A, Conti CJ, Deng CX, Jorcano JL, and Johnson DG (2003). Tumor formation in mice with conditional inactivation of Brca1 in epithelial tissues. Oncogene 22, 5415–5426. [PubMed: 12934101]

Bohgaki T, Bohgaki M, Cardoso R, Panier S, Zeegers D, Li L, Stewart GS, Sanchez O, Hande MP, Durocher D, et al. (2011). Genomic instability, defective spermatogenesis, immunodeficiency, and cancer in a mouse model of the RIDDLE syndrome. PLoS Genet 7, e1001381. [PubMed: 21552324]

Bouwman P, Aly A, Escandell JM, Pieterse M, Bartkova J, van der Gulden H, Hiddingh S, Thanasoula M, Kulkarni A, Yang Q, et al. (2010). 53BP1 loss rescues BRCA1 deficiency and is associated with triple-negative and BRCA-mutated breast cancers. Nat Struct Mol Biol 17, 688–695. [PubMed: 20453858]

Bowman-Colin C, Xia B, Bunting S, Klijn C, Drost R, Bouwman P, Fineman L, Chen X, Culhane AC, Cai H, et al. (2013). Palb2 synergizes with Trp53 to suppress mammary tumor formation in a model of inherited breast cancer. Proc Natl Acad Sci U S A 110, 8632–8637. [PubMed: 23657012]

Bunting SF, Callen E, Wong N, Chen HT, Polato F, Gunn A, Bothmer A, Feldhahn N, FernandezCapetillo O, Cao L, et al. (2010). 53BP1 inhibits homologous recombination in Brca1-deficient cells by blocking resection of DNA breaks. Cell 141, 243–254. [PubMed: 20362325]

Bunting SF, and Nussenzweig A (2013). End-joining, translocations and cancer. Nat Rev Cancer 13, 443–454. [PubMed: 23760025]

Callen E, Di Virgilio M, Kruhlak MJ, Nieto-Soler M, Wong N, Chen HT, Faryabi RB, Polato F, Santos M, Starnes LM, et al. (2013). 53BP1 mediates productive and mutagenic DNA repair through distinct phosphoprotein interactions. Cell 153, 1266–1280. [PubMed: 23727112]

Cao L, Xu X, Bunting SF, Liu J, Wang RH, Cao LL, Wu JJ, Peng TN, Chen J, Nussenzweig A, et al. (2009). A selective requirement for 53BP1 in the biological response to genomic instability induced by Brca1 deficiency. Mol Cell 35, 534–541. [PubMed: 19716796]

Celeste A, Fernandez-Capetillo O, Kruhlak MJ, Pilch DR, Staudt DW, Lee A, Bonner RF, Bonner WM, and Nussenzweig A (2003). Histone H2AX phosphorylation is dispensable for the initial recognition of DNA breaks. Nat Cell Biol 5, 675–679. [PubMed: 12792649]

Celeste A, Petersen S, Romanienko PJ, Fernandez-Capetillo O, Chen HT, Sedelnikova OA, Reina-San-Martin B, Coppola V, Meffre E, Difilippantonio MJ, et al. (2002). Genomic instability in mice lacking histone H2AX. Science 296, 922–927. [PubMed: 11934988]

Chen CC, Kass EM, Yen WF, Ludwig T, Moynahan ME, Chaudhuri J, and Jasin M (2017). ATM loss leads to synthetic lethality in BRCA1 BRCT mutant mice associated with exacerbated defects in homology-directed repair. Proc Natl Acad Sci U S A 114, 7665–7670. [PubMed: 28659469]

Coleman KA, and Greenberg RA (2011). The BRCA1-RAP80 complex regulates DNA repair mechanism utilization by restricting end resection. J Biol Chem 286, 13669–13680. [PubMed: 21335604]

Cuadrado M, Martinez-Pastor B, Murga M, Toledo LI, Gutierrez-Martinez P, Lopez E, and Fernandez-Capetillo O (2006). ATM regulates ATR chromatin loading in response to DNA double-strand breaks. J Exp Med 203, 297–303. [PubMed: 16461339]

Di Virgilio M, Callen E, Yamane A, Zhang W, Jankovic M, Gitlin AD, Feldhahn N, Resch W, Oliveira TY, Chait BT, et al. (2013). Rif1 prevents resection of DNA breaks and promotes immunoglobulin class switching. Science 339, 711–715. [PubMed: 23306439]

Doil C, Mailand N, Bekker-Jensen S, Menard P, Larsen DH, Pepperkok R, Ellenberg J, Panier S, Durocher D, Bartek J, et al. (2009). RNF168 binds and amplifies ubiquitin conjugates on damaged chromosomes to allow accumulation of repair proteins. Cell 136, 435–446. [PubMed: 19203579]

Drost R, Dhillon KK, van der Gulden H, van der Heijden I, Brandsma I, Cruz C, Chondronasiou D, Castroviejo-Bermejo M, Boon U, Schut E, et al. (2016). BRCA1185delAG tumors may acquire therapy resistance through expression of RING-less BRCA1. J Clin Invest 126, 2903–2918. [PubMed: 27454287]

Escribano-Diaz C, Orthwein A, Fradet-Turcotte A, Xing M, Young JT, Tkac J, Cook MA, Rosebrock AP, Munro M, Canny MD, et al. (2013). A cell cycle-dependent regulatory circuit composed of 53BP1-RIF1 and BRCA1-CtIP controls DNA repair pathway choice. Mol Cell 49, 872–883. [PubMed: 23333306]

Feng L, Fong KW, Wang J, Wang W, and Chen J (2013). RIF1 counteracts BRCA1-mediated end resection during DNA repair. J Biol Chem 288, 11135–11143. [PubMed: 23486525]

Gu Y, Bouwman P, Greco D, Saarela J, Yadav B, Jonkers J, and Kuznetsov SG (2014). Suppression of BRCA1 sensitizes cells to proteasome inhibitors. Cell Death Dis 5, e1580. [PubMed: 25522274]

Gudjonsson T, Altmeyer M, Savic V, Toledo L, Dinant C, Grofte M, Bartkova J, Poulsen M, Oka Y, Bekker-Jensen S, et al. (2012). TRIP12 and UBR5 suppress spreading of chromatin ubiquitylation at damaged chromosomes. Cell 150, 697–709. [PubMed: 22884692]

Hu Y, Scully R, Sobhian B, Xie A, Shestakova E, and Livingston DM (2011). RAP80-directed tuning of BRCA1 homologous recombination function at ionizing radiation-induced nuclear foci. Genes Dev 25, 685–700. [PubMed: 21406551]

Huang TH, Fowler F, Chen CC, Shen ZJ, Sleckman B, and Tyler JK (2018). The Histone Chaperones ASF1 and CAF-1 Promote MMS22L-TONSL-Mediated Rad51 Loading onto ssDNA during Homologous Recombination in Human Cells. Mol Cell 69, 879–892 e875. [PubMed: 29478807]

Huen MS, Grant R, Manke I, Minn K, Yu X, Yaffe MB, and Chen J (2007). RNF8 transduces the DNA-damage signal via histone ubiquitylation and checkpoint protein assembly. Cell 131, 901–914. [PubMed: 18001825]

Jazayeri A, Falck J, Lukas C, Bartek J, Smith GC, Lukas J, and Jackson SP (2006). ATM- and cell cycle-dependent regulation of ATR in response to DNA double-strand breaks. Nat Cell Biol 8, 37–45. [PubMed: 16327781]

Kinzler KW, and Vogelstein B (1997). Cancer-susceptibility genes. Gatekeepers and caretakers. Nature 386, 761, 763. [PubMed: 9126728]

Kolas NK, Chapman JR, Nakada S, Ylanko J, Chahwan R, Sweeney FD, Panier S, Mendez M, Wildenhain J, Thomson TM, et al. (2007). Orchestration of the DNA-damage response by the RNF8 ubiquitin ligase. Science 318, 1637–1640. [PubMed: 18006705]

Li M, Cole F, Patel DS, Misenko SM, Her J, Malhowski A, Alhamza A, Zheng H, Baer R, Ludwig T, et al. (2016). 53BP1 ablation rescues genomic instability in mice expressing 'RING-less' BRCA1. EMBO Rep 17, 1532–1541. [PubMed: 27670884]

Li ML, and Greenberg RA (2012). Links between genome integrity and BRCA1 tumor suppression. Trends Biochem Sci 37, 418–424. [PubMed: 22836122]

Ludwig T, Chapman DL, Papaioannou VE, and Efstratiadis A (1997). Targeted mutations of breast cancer susceptibility gene homologs in mice: lethal phenotypes of Brca1, Brca2, Brca1/Brca2, Brca1/p53, and Brca2/p53 nullizygous embryos. Genes Dev 11, 1226–1241. [PubMed: 9171368]

Luijsterburg MS, Typas D, Caron MC, Wiegant WW, van den Heuvel D, Boonen RA, Couturier AM, Mullenders LH, Masson JY, and van Attikum H (2017). A PALB2-interacting domain in RNF168 couples homologous recombination to DNA break-induced chromatin ubiquitylation. Elife 6.

Mailand N, Bekker-Jensen S, Faustrup H, Melander F, Bartek J, Lukas C, and Lukas J (2007). RNF8 ubiquitylates histones at DNA double-strand breaks and promotes assembly of repair proteins. Cell 131, 887–900. [PubMed: 18001824]

Manis JP, Morales JC, Xia Z, Kutok JL, Alt FW, and Carpenter PB (2004). 53BP1 links DNA damage-response pathways to immunoglobulin heavy chain class-switch recombination. Nat Immunol 5, 481–487. [PubMed: 15077110]

Mattiroli F, Vissers JH, van Dijk WJ, Ikpa P, Citterio E, Vermeulen W, Marteijn JA, and Sixma TK (2012). RNF168 ubiquitinates K13–15 on H2A/H2AX to drive DNA damage signaling. Cell 150, 1182–1195. [PubMed: 22980979]

Messick TE, and Greenberg RA (2009). The ubiquitin landscape at DNA double-strand breaks. J Cell Biol 187, 319–326. [PubMed: 19948475]

Munoz MC, Laulier C, Gunn A, Cheng A, Robbiani DF, Nussenzweig A, and Stark JM (2012). RING finger nuclear factor RNF168 is important for defects in homologous recombination caused by loss of the breast cancer susceptibility factor BRCA1. J Biol Chem 287, 40618–40628. [PubMed: 23055523]

Nakada S, Yonamine RM, and Matsuo K (2012). RNF8 regulates assembly of RAD51 at DNA double-strand breaks in the absence of BRCA1 and 53BP1. Cancer Res 72, 4974–4983. [PubMed: 22865450]

Nikkila J, Parplys AC, Pylkas K, Bose M, Huo Y, Borgmann K, Rapakko K, Nieminen P, Xia B, Pospiech H, et al. (2013). Heterozygous mutations in PALB2 cause DNA replication and damage response defects. Nat Commun 4, 2578. [PubMed: 24153426]

Noordermeer SM, Adam S, Setiaputra D, Barazas M, Pettitt SJ, Ling AK, Olivieri M, Alvarez-Quilon A, Moatti N, Zimmermann M, et al. (2018). The shieldin complex mediates 53BP1-dependent DNA repair. Nature 560, 117–121. [PubMed: 30022168]

Orthwein A, Noordermeer SM, Wilson MD, Landry S, Enchev RI, Sherker A, Munro M, Pinder J, Salsman J, Dellaire G, et al. (2015). A mechanism for the suppression of homologous recombination in G1 cells. Nature 528, 422–426. [PubMed: 26649820]

Pathania S, Bade S, Le Guillou M, Burke K, Reed R, Bowman-Colin C, Su Y, Ting DT, Polyak K, Richardson AL, et al. (2014). BRCA1 haploinsufficiency for replication stress suppression in primary cells. Nat Commun 5, 5496. [PubMed: 25400221]

Peterson SE, Li Y, Wu-Baer F, Chait BT, Baer R, Yan H, Gottesman ME, and Gautier J (2013). Activation of DSB processing requires phosphorylation of CtIP by ATR. Mol Cell 49, 657–667. [PubMed: 23273981]

Pilch DR, Sedelnikova OA, Redon C, Celeste A, Nussenzweig A, and Bonner WM (2003). Characteristics of gamma-H2AX foci at DNA double-strand breaks sites. Biochem Cell Biol 81, 123–129. [PubMed: 12897845]

Polato F, Callen E, Wong N, Faryabi R, Bunting S, Chen HT, Kozak M, Kruhlak MJ, Reczek CR, Lee WH, et al. (2014). CtIP-mediated resection is essential for viability and can operate independently of BRCA1. J Exp Med 211, 1027–1036. [PubMed: 24842372]

Prakash R, Zhang Y, Feng W, and Jasin M (2015). Homologous recombination and human health: the roles of BRCA1, BRCA2, and associated proteins. Cold Spring Harb Perspect Biol 7, a016600. [PubMed: 25833843]

Rantakari P, Nikkila J, Jokela H, Ola R, Pylkas K, Lagerbohm H, Sainio K, Poutanen M, and Winqvist R (2010). Inactivation of Palb2 gene leads to mesoderm differentiation defect and early embryonic lethality in mice. Hum Mol Genet 19, 3021–3029. [PubMed: 20484223]

Ray Chaudhuri A, Callen E, Ding X, Gogola E, Duarte AA, Lee JE, Wong N, Lafarga V, Calvo JA, Panzarino NJ, et al. (2016). Replication fork stability confers chemoresistance in BRCA-deficient cells. Nature 535, 382–387. [PubMed: 27443740]

Santos MA, Huen MS, Jankovic M, Chen HT, Lopez-Contreras AJ, Klein IA, Wong N, Barbancho JL, Fernandez-Capetillo O, Nussenzweig MC, et al. (2010). Class switching and meiotic defects in mice lacking the E3 ubiquitin ligase RNF8. J Exp Med 207, 973–981. [PubMed: 20385748]

Sasanuma H, Tsuda M, Morimoto S, Saha LK, Rahman MM, Kiyooka Y, Fujiike H, Cherniack AD, Itou J, Callen Moreu E, et al. (2018). BRCA1 ensures genome integrity by eliminating estrogen-induced pathological topoisomerase II-DNA complexes. Proc Natl Acad Sci U S A 115, E10642–E10651. [PubMed: 30352856]

Sedic M, and Kuperwasser C (2016). BRCA1-hapoinsufficiency: Unraveling the molecular and cellular basis for tissue-specific cancer. Cell Cycle 15, 621–627. [PubMed: 26822887]

Shiotani B, and Zou L (2009). Single-stranded DNA orchestrates an ATM-to-ATR switch at DNA breaks. Mol Cell 33, 547–558. [PubMed: 19285939]

Simhadri S, Peterson S, Patel DS, Huo Y, Cai H, Bowman-Colin C, Miller S, Ludwig T, Ganesan S, Bhaumik M, et al. (2014). Male fertility defect associated with disrupted BRCA1-PALB2 interaction in mice. J Biol Chem 289, 24617–24629. [PubMed: 25016020]

Stewart GS, Panier S, Townsend K, Al-Hakim AK, Kolas NK, Miller ES, Nakada S, Ylanko J, Olivarius S, Mendez M, et al. (2009). The RIDDLE syndrome protein mediates a ubiquitin-dependent signaling cascade at sites of DNA damage. Cell 136, 420–434. [PubMed: 19203578]

Stucki M, Clapperton JA, Mohammad D, Yaffe MB, Smerdon SJ, and Jackson SP (2005). MDC1 directly binds phosphorylated histone H2AX to regulate cellular responses to DNA double-strand breaks. Cell 123, 1213–1226. [PubMed: 16377563]

Sy SM, Huen MS, and Chen J (2009). PALB2 is an integral component of the BRCA complex required for homologous recombination repair. Proc Natl Acad Sci U S A 106, 7155–7160. [PubMed: 19369211]

Tan SLW, Chadha S, Liu Y, Gabasova E, Perera D, Ahmed K, Constantinou S, Renaudin X, Lee M, Aebersold R, et al. (2017). A Class of Environmental and Endogenous Toxins Induces BRCA2 Haploinsufficiency and Genome Instability. Cell 169, 1105–1118 e1115. [PubMed: 28575672]

Thorslund T, Ripplinger A, Hoffmann S, Wild T, Uckelmann M, Villumsen B, Narita T, Sixma TK, Choudhary C, Bekker-Jensen S, et al. (2015). Histone H1 couples initiation and amplification of ubiquitin signalling after DNA damage. Nature 527, 389–393. [PubMed: 26503038]

Tutt A, and Ashworth A (2002). The relationship between the roles of BRCA genes in DNA repair and cancer predisposition. Trends Mol Med 8, 571–576. [PubMed: 12470990]

Wang Y, Bernhardy AJ, Cruz C, Krais JJ, Nacson J, Nicolas E, Peri S, van der Gulden H, van der Heijden I, O'Brien SW, et al. (2016a). The BRCA1-Delta11q Alternative Splice Isoform Bypasses Germline Mutations and Promotes Therapeutic Resistance to PARP Inhibition and Cisplatin. Cancer Res 76, 2778–2790. [PubMed: 27197267]

Wang Y, Krais JJ, Bernhardy AJ, Nicolas E, Cai KQ, Harrell MI, Kim HH, George E, Swisher EM, Simpkins F, et al. (2016b). RING domain-deficient BRCA1 promotes PARP inhibitor and platinum resistance. J Clin Invest 126, 3145–3157. [PubMed: 27454289]

Ward IM, Minn K, van Deursen J, and Chen J (2003). p53 Binding protein 53BP1 is required for DNA damage responses and tumor suppression in mice. Mol Cell Biol 23, 2556–2563. [PubMed: 12640136]

Ward IM, Reina-San-Martin B, Olaru A, Minn K, Tamada K, Lau JS, Cascalho M, Chen L, Nussenzweig A, Livak F, et al. (2004). 53BP1 is required for class switch recombination. J Cell Biol 165, 459–464. [PubMed: 15159415]

Wilson MD, Benlekbir S, Fradet-Turcotte A, Sherker A, Julien JP, McEwan A, Noordermeer SM, Sicheri F, Rubinstein JL, and Durocher D (2016). The structural basis of modified nucleosome recognition by 53BP1. Nature 536, 100–103. [PubMed: 27462807]

Xie A, Hartlerode A, Stucki M, Odate S, Puget N, Kwok A, Nagaraju G, Yan C, Alt FW, Chen J, et al. (2007). Distinct roles of chromatin-associated proteins MDC1 and 53BP1 in mammalian double-strand break repair. Mol Cell 28, 1045–1057. [PubMed: 18158901]

Xie A, Puget N, Shim I, Odate S, Jarzyna I, Bassing CH, Alt FW, and Scully R (2004). Control of sister chromatid recombination by histone H2AX. Mol Cell 16, 1017–1025. [PubMed: 15610743]

Xu X, Qiao W, Linke SP, Cao L, Li WM, Furth PA, Harris CC, and Deng CX (2001). Genetic interactions between tumor suppressors Brca1 and p53 in apoptosis, cell cycle and tumorigenesis. Nat Genet 28, 266–271. [PubMed: 11431698]

Yazinski SA, Comaills V, Buisson R, Genois MM, Nguyen HD, Ho CK, Todorova Kwan T, Morris R, Lauffer S, Nussenzweig A, et al. (2017). ATR inhibition disrupts rewired homologous recombination and fork protection pathways in PARP inhibitor-resistant BRCA-deficient cancer cells. Genes Dev 31, 318–332. [PubMed: 28242626]

Zhang F, Bick G, Park JY, and Andreassen PR (2012). MDC1 and RNF8 function in a pathway that directs BRCA1-dependent localization of PALB2 required for homologous recombination. J Cell Sci 125, 6049–6057. [PubMed: 23038782]

Zhang F, Fan Q, Ren K, and Andreassen PR (2009a). PALB2 functionally connects the breast cancer susceptibility proteins BRCA1 and BRCA2. Mol Cancer Res 7, 1110–1118. [PubMed: 19584259]

Zhang F, Ma J, Wu J, Ye L, Cai H, Xia B, and Yu X (2009b). PALB2 links BRCA1 and BRCA2 in the DNA-damage response. Curr Biol 19, 524–529. [PubMed: 19268590]

Zimmermann M, Lottersberger F, Buonomo SB, Sfeir A, and de Lange T (2013). 53BP1 regulates DSB repair using Rif1 to control 5' end resection. Science 339, 700–704. [PubMed: 23306437]

Zong D, Callen E, Pegoraro G, Lukas C, Lukas J, and Nussenzweig A (2015). Ectopic expression of RNF168 and 53BP1 increases mutagenic but not physiological non-homologous end joining. Nucleic Acids Res 43, 4950–4961. [PubMed: 25916843]

Highlights

- The E3 ubiquitin ligase RNF168 supports BRCA1-independent homologous recombination
- RNF168 acts redundantly with BRCA1 to load PALB2 onto damaged DNA
- Targeting RNF168 could induce synthetic lethality in BRCA1-deficient cancers
- The function of BRCA1 in replication fork protection is separable from its role HR

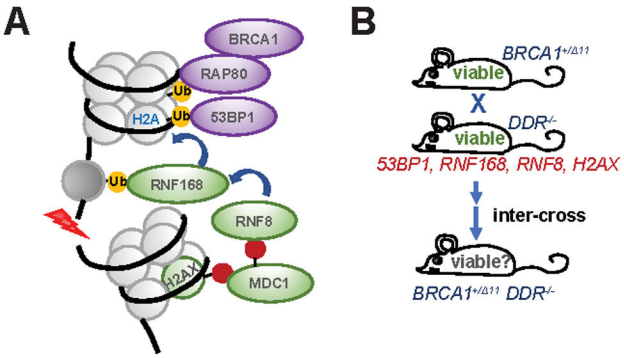

C

BRCA1	53BP1	Expected	Observed	P value
+/+	+/-	10	15	n.s.
+/+	-/-	5	6	n.s.
Δ11/Δ11	+/-	10	0	0.0007
Δ11/Δ11	-/-	5	9	n.s.
Total number of live pups: 81				

D

BRCA1	RNF168	Expected	Observed	P value
+/+	+/+, +/-	32	54	<0.0001
+/+	-/-	11	12	n.s.
Δ11/Δ11	+/+, +/-	32	0	<0.0001
Δ11/Δ11	-/-	11	0	0.0008
Total number of live pups: 170				

E

53BP1	BRCA1	RNF168	Expected	Observed	P value
-/-	+/+	+/+, +/-	33	40	n.s.
-/-	+/+	-/-	11	7	n.s.
-/-	Δ11/Δ11	+/+, +/-	33	45	0.02
-/-	Δ11/Δ11	-/-	11	0	0.0007
Total number of live pups: 262					

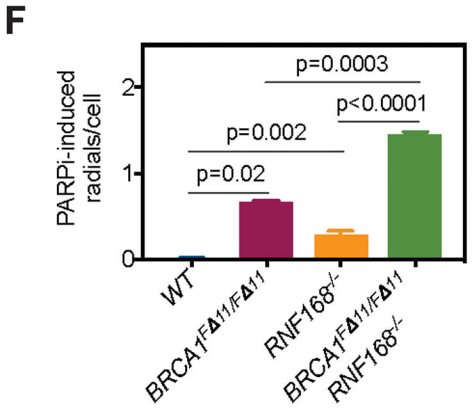

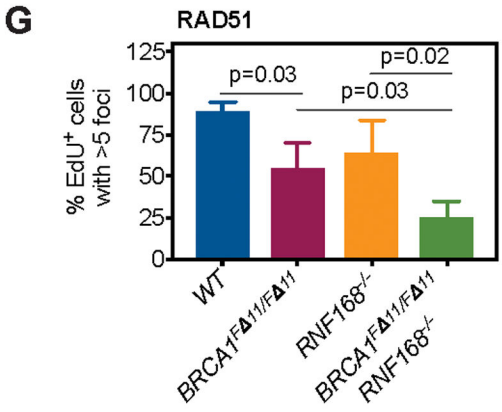

Figure 1. RNF168 sustains organismal viability and genome maintenance when *BRCA1* is inactivated.

(**A**) Model of the γ-H2AX-RNF8-RNF168 chromatin ubiquitylation pathway and downstream effectors.

(**B**) Breeding strategy to generate mice with combined deficiencies in *BRCA1* and the DNA damage response (DDR) factors *H2AX, RNF8, RNF168* or *53BP1.*

(**C-E**) Summary of breeding outcomes from the $BRCA1^{+/\Delta11}53BP1^{+/-}$ X $BRCA1^{+/\Delta11}53BP1^{-/-}$ intercross (C), the $BRCA1^{+/\Delta11}RNF168^{+/-}$ X $BRCA1^{+/\Delta11}RNF168^{+/-}$ intercross (D), and three intercrosses: $BRCA1^{+/\Delta11}RNF168^{+/-}53BP1^{+/-}$ X $BRCA1^{+/\Delta11}RNF168^{+/-}53BP1^{+/-}$; $BRCA1^{+/\Delta11}RNF168^{+/-}53BP1^{+/-}$ X $BRCA1^{+/\Delta11}RNF168^{+/-}53BP1^{-/-}$; $BRCA1^{+/\Delta11}RNF168^{+/-}53BP1^{-/-}$ X $BRCA1^{+/\Delta11}RNF168^{+/-}53BP1^{-/-}$ (E).

(**F**) The average number of chromosomal radials per metaphase spread in *WT,* $BRCA1^{F\Delta11/F\Delta11;\ CD19Cre}$ $RNF168^{-/-}$ and $BRCA1^{F\Delta11/F\Delta11;\ CD19Cre}$ $RNF168^{-/-}$ B cells exposed to PARPi.

(**G**) The percentage of EdU-positive (S-phase) *WT*, *BRCA1*$^{FΔ11/FΔ11;\ CD19Cre}$, *RNF168*$^{-/-}$ and *BRCA1*$^{FΔ11/FΔ11;\ CD19Cre}$ *RNF168*$^{-/-}$ B cells that stained positive for RAD51 foci 4 hours post γ-irradiation (5 Gy). Data in F and G are presented as mean ± SD. In C-E and F-G, statistical significance was calculated using χ^2 test for goodness of fit and unpaired two-tailed Student's *t*-test, respectively. See also Figures S1 and S2.

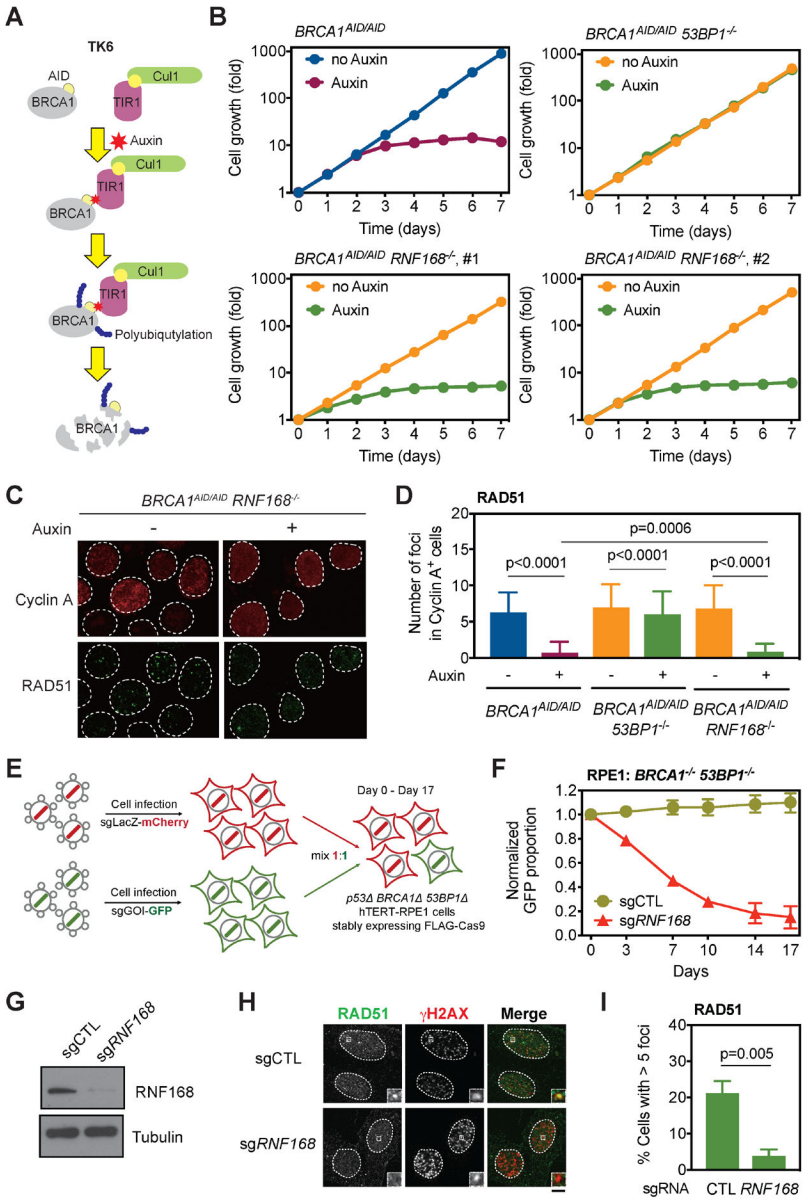

Figure 2. RNF168 supports BRCA1-independent survival in human cells.

(**A**) The auxin-induced BRCA1 degradation system in human TK6 cells.

(**B**) The growth profile of *BRCA1*$^{AID/AID}$, *BRCA1*$^{AID/AID}$*53BP1*$^{-/-}$ and *BRCA1*$^{AID/AID}$*RNF168*$^{-/-}$ TK6 cells in the absence and presence of 0.5 mM auxin. BRCA1 degradation induced by addition of auxin resulted in severe growth inhibition in both *BRCA1*$^{AID/AID}$ and two independent clones of *BRCA1*$^{AID/AID}$*RNF168*$^{-/-}$ TK6 cells ($p<0.0001$ compared to no auxin). Loss of 53BP1 rescued the growth defect in BRCA1-depleted cells.

(**C**) RAD51 foci formation in *BRCA1*$^{AID/AID}$, *BRCA1*$^{AID/AID}$*53BP1*$^{-/-}$ and *BRCA1*$^{AID/AID}$*RNF168*$^{-/-}$ TK6 cells 2 hours post γ-irradiation (2 Gy); cells were pre-treated or not with 0.5 mM auxin.

(**D**) The average number of RAD51 foci per cell among irradiated Cyclin A-positive (S/G2) TK6 cells.

(**E**) Outline of the Multicolor Competition Assay (MCA).

(**F**) MCA in *Cas9*$^{+}$*BRCA1*$^{-/-}$*53BP1*$^{-/-}$ human hTERT-RPE1 cells transduced with a specific guide RNA targeting *RNF168* or an empty vector (sgCTL). RPE1 cells transduced non-targeting guides (sgLacZ) were used as the competitor. Deletion of *RNF168* significantly attenuated the growth of *BRCA1*$^{-/-}$ *53BP1*$^{-/-}$ cells following PARPi treatment ($p<0.0001$).

(**G**) Efficient knockdown of RNF168 in *BRCA1*$^{-/-}$*53BP1*$^{-/-}$ hTERT-RPE1 cells by CRISPR-Cas9. A representative blot is shown.

(**H**) RAD51 foci formation in *BRCA1*$^{-/-}$*53BP1*$^{-/-}$ hTERT-RPE1 cells transduced with either sgCTL or sg*RNF168* 4 hours post γ-irradiation (5 Gy).

(**I**) The percentage of *BRCA1*$^{-/-}$*53BP1*$^{-/-}$ hTERT-RPE1 cells stained positive for RAD51 foci 4 hours post γ-irradiation (5 Gy).

Data in B, D, F and I are presented as mean ± SD. In B/F, D and I, statistical significance was calculated using two-way ANOVA, Mann-Whitney test and two-tailed Student's *t*-test, respectively. See also Figure S3.

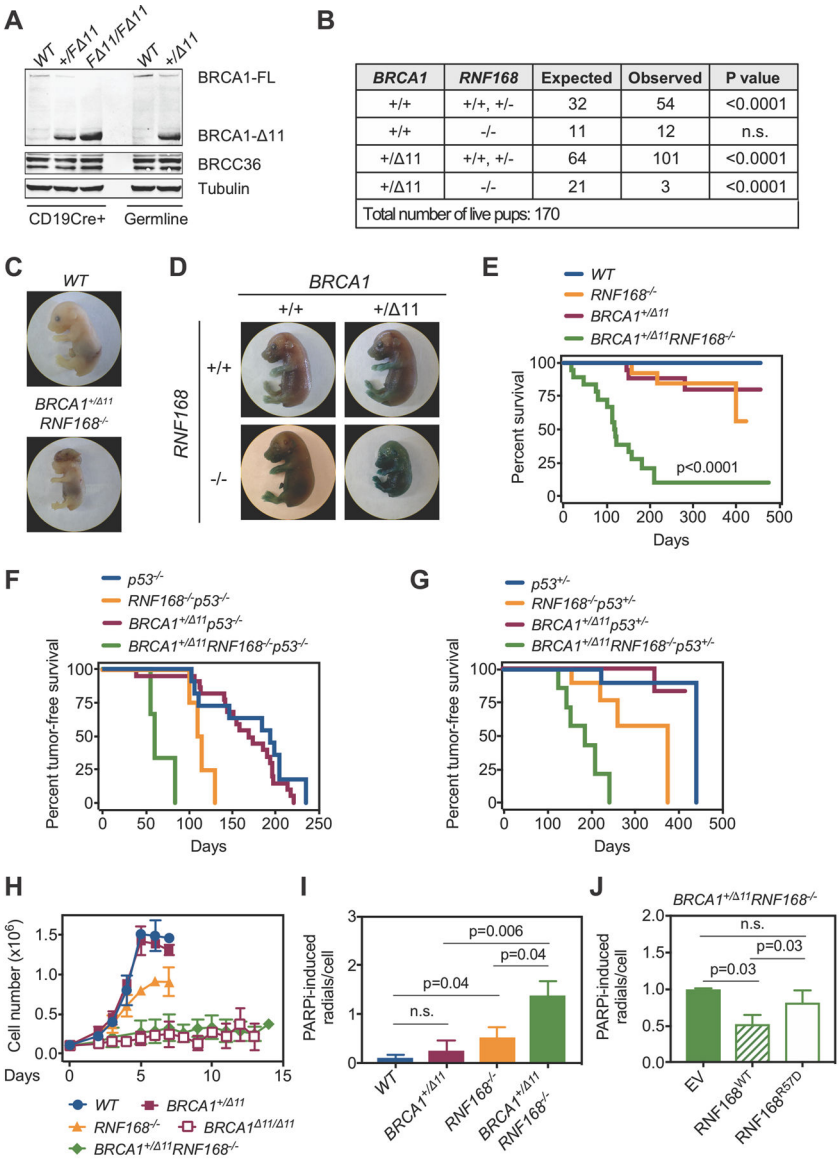

BRCA1	RNF168	Expected	Observed	P value
+/+	+/+, +/-	32	54	<0.0001
+/+	-/-	11	12	n.s.
+/Δ11	+/+, +/-	64	101	<0.0001
+/Δ11	-/-	21	3	<0.0001
Total number of live pups: 170				

Figure 3. Loss of *RNF168* unmasks *BRCA1* haploinsufficiency.

(**A**) BRCA1 protein expression level (full-length and delta-11 isoforms) in *BRCA1* heterozygous cells (*BRCA1+/Δ11* and *BRCA1+/FΔ11; CD19Cre*); *WT* and *BRCA1FΔ11/FΔ11; CD19Cre* cells were used as controls.

(**B**) Summary of breeding outcomes from the $BRCA1^{+/\Delta11}RNF168^{+/-}$ X $BRCA1^{+/\Delta11}RNF168^{+/-}$ intercross.

(**C**) Representative morphology of E16.5 *WT* and $BRCA1^{+/\Delta11}RNF168^{-/-}$ embryos; the latter exhibited growth retardation as well as exencephaly.

(**D**) Staining of E16.5 embryos for senescence-associated β-galactosidase activity.

(**E**) Kaplan-Meier survival analysis of *WT* (n=8), $BRCA1^{+/\Delta11}$ (n=16), $RNF168^{-/-}$ (n=13) and $BRCA1^{+/\Delta11}RNF168^{-/-}$ (n=19) mice. Significantly shorter lifespan was observed in $BRCA1^{+/\Delta11}RNF168^{-/-}$ mice compared to the $RNF168^{-/-}$ counterparts (p<0.0001).

(**F**) Kaplan-Meier survival analysis of $p53^{-/-}$ (n=11), $BRCA1^{+/\Delta 11}p53^{-/-}$ (n=22), $RNF168^{-/-}p53^{-/-}$ (n=4) and $BRCA1^{+/\Delta 11}RNF168^{-/-}p53^{-/-}$ (n=3) mice. Significantly shorter tumor-free survival was observed in $BRCA1^{+/\Delta 11}RNF168^{-/-}p53^{-/-}$ mice compared to $BRCA1^{+/\Delta 11}p53^{-/-}$ and $RNF168^{-/-}p53^{-/-}$ counterparts ($p<0.0001$ and $p=0.01$, respectively).

(**G**) Kaplan-Meier survival analysis of $p53^{+/-}$ (n=10), $BRCA1^{+/\Delta 11}p53^{+/-}$ (n=11), $RNF168^{-/-}p53^{+/-}$ (n=10) and $BRCA1^{+/\Delta 11}RNF168^{-/-}p53^{+/-}$ (n=8) mice. Significantly shorter tumor-free survival was observed in $BRCA1^{+/\Delta 11}RNF168^{-/-}p53^{+/-}$ mice compared to $BRCA1^{+/\Delta 11}p53^{-/-}$ and $RNF168^{-/-}p53^{-/-}$ counterparts ($p<0.0001$ and $p=0.003$, respectively).

(**H**) Growth of *WT*, $BRCA1^{+/\Delta 11}$, $RNF168^{-/-}$ and $BRCA1^{+/\Delta 11}RNF168^{-/-}$ primary mouse embryonic fibroblasts (MEFs) in culture. $BRCA1^{+/\Delta 11}RNF168^{-/-}$ cells grew significantly slower than $BRCA1^{+/\Delta 11}$ and $RNF168^{-/-}$ counterparts ($p=0.02$, Kruskal-Wallis test).

(**I**) The average number of chromosomal radials per metaphase spread in *WT*, $BRCA1^{+/\Delta 11}$, $RNF168^{-/-}$ and $BRCA1^{+/\Delta 11}RNF168^{-/-}$ MEFs exposed to PARPi.

(**J**) The average number of chromosomal radials per metaphase spread in PARPi-treated $BRCA1^{+/\Delta 11}RNF168^{-/-}$ MEFs stably expressing WT or catalytic mutant (R57D) forms of RNF168. $BRCA1^{+/\Delta 11}RNF168^{-/-}$ MEFs transduced with empty vector (EV) were used as control.

Data in G-I are presented as mean ± SD. In B and H, statistical significance was calculated using χ^2 test for goodness of fit and one-way ANOVA, respectively. In E-G and I-J, statistical significance was calculated using Mantel-Cox test and unpaired two-tailed Student's *t*-test, respectively. See also Figure S4 and S5.

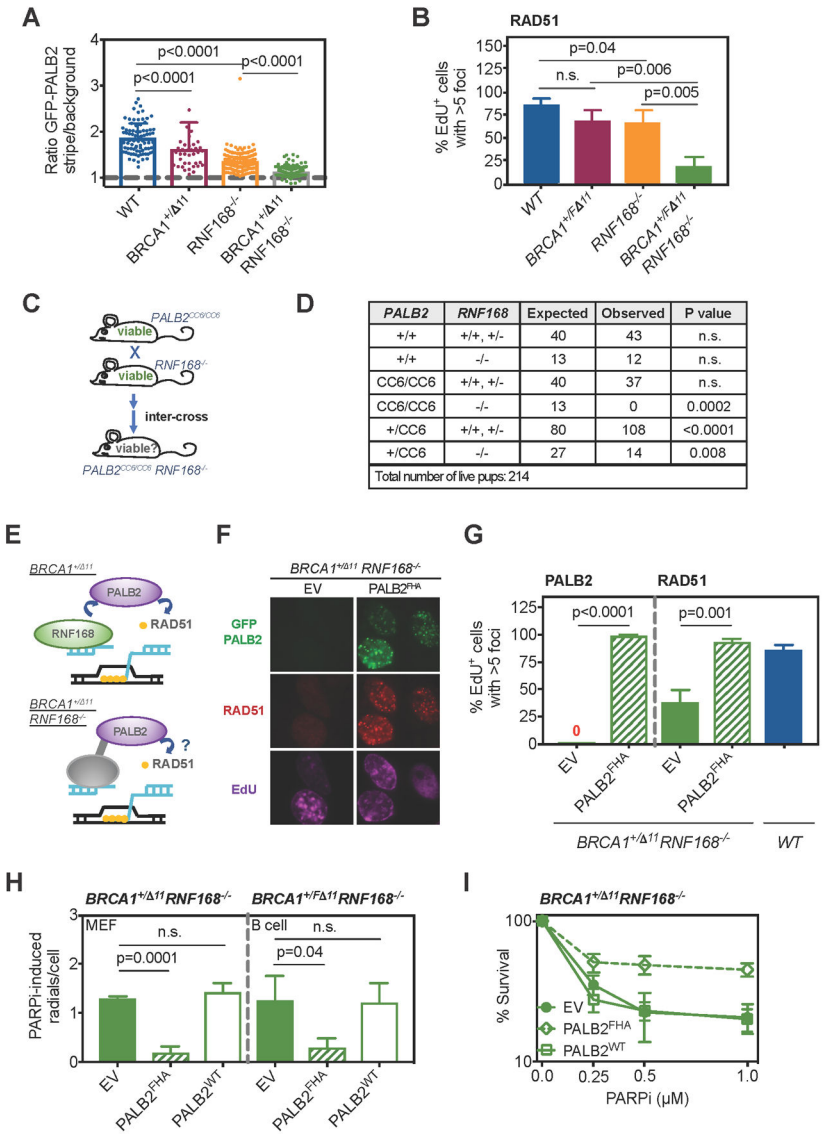

PALB2	RNF168	Expected	Observed	P value
+/+	+/+, +/-	40	43	n.s.
+/+	-/-	13	12	n.s.
CC6/CC6	+/+, +/-	40	37	n.s.
CC6/CC6	-/-	13	0	0.0002
+/CC6	+/+, +/-	80	108	<0.0001
+/CC6	-/-	27	14	0.008
Total number of live pups: 214				

Figure 4. RNF168-mediated PALB2 recruitment is essential for viability and genome maintenance when the BRCA1-PALB2 pathway is compromised.

(**A**) The average fluorescence intensity of PALB2 stripes in *WT*, *BRCA1*$^{+/\Delta 11}$, *RNF168*$^{-/-}$ and *BRCA1*$^{+/\Delta 11}$*RNF168*$^{-/-}$ MEFs stably expressing GFP-PALB2. Signals were normalized to the background noise.

(**B**) The percentage of EdU-positive (S-phase) *WT*, *BRCA1*$^{+/F\Delta 11;\ CD19Cre}$, *RNF168*$^{-/-}$ and *BRCA1*$^{+/F\Delta 11;}$ CD19Cre *RNF168*$^{-/-}$ B cells that stained positive for RAD51 foci 4 hours post γ-irradiation (5 Gy).

(**C**) Breeding strategy for the generation of mice lacking *RNF168* in the context of an abrogated BRCA1-PALB2 interaction (*PALB2*^{CC6}).

(**D**) Summary of breeding outcomes from the *PALB2*$^{+/CC6}$*RNF168*$^{+/-}$ X *PALB2*$^{+/CC6}$*RNF168*$^{+/-}$ intercross.

(**E**) Strategy for forced targeting of PALB2 to DSB sites.

(**F**) Formation of PALB2 and RAD51 foci in *BRCA1*$^{+/\Delta 11}$*RNF168*$^{-/-}$ MEFs stably expressing GFP-PALB2^{FHA}.

(**G**) The percentage of EdU-positive (S-phase) *BRCA1*$^{+/\Delta 11}$*RNF168*$^{-/-}$ MEFs stably expressing GFP-PALB2^{FHA} that stained positive for PALB2 and RAD51 foci 4 hours post γ-irradiation (10 Gy). *WT* MEFs and *BRCA1*$^{+/\Delta 11}$*RNF168*$^{-/-}$ MEFs transduced with empty vector (EV) were used as controls.

(**H**) The average number of chromosomal radials per metaphase spread in PARPi-treated *BRCA1*$^{+/\Delta}$*11RNF168*$^{-/-}$ MEFs and *BRCA1*$^{+/F\Delta 11;\ CD19Cre}$ *RNF168*$^{-/-}$ B cells stably expressing WT PALB2 or PALB2^{FHA}.

(**I**) Colony formation capacity of *BRCA1*$^{+/\Delta 11}$*RNF168*$^{-/-}$ MEFs stably expressing WT PALB2 or PALB2^{FHA} after treatment with PARPi. PALB2^{FHA} expression significantly rescued PARPi hypersensitivity in *BRCA1*$^{+/\Delta 11}$*RNF168*$^{-/-}$ MEFs ($p<0.0001$). In H and I, MEFs and B cells transduced with empty vector (EV) were used as controls.

Data in A, B and G-I are presented as mean ± SD. In A and D, statistical significance was calculated using Mann-Whitney test and χ^2 test for goodness of fit, respectively. In G-H and I, statistical significance was calculated using unpaired two-tailed Student's *t*-test and two-way ANOVA, respectively. See also Figure S6.

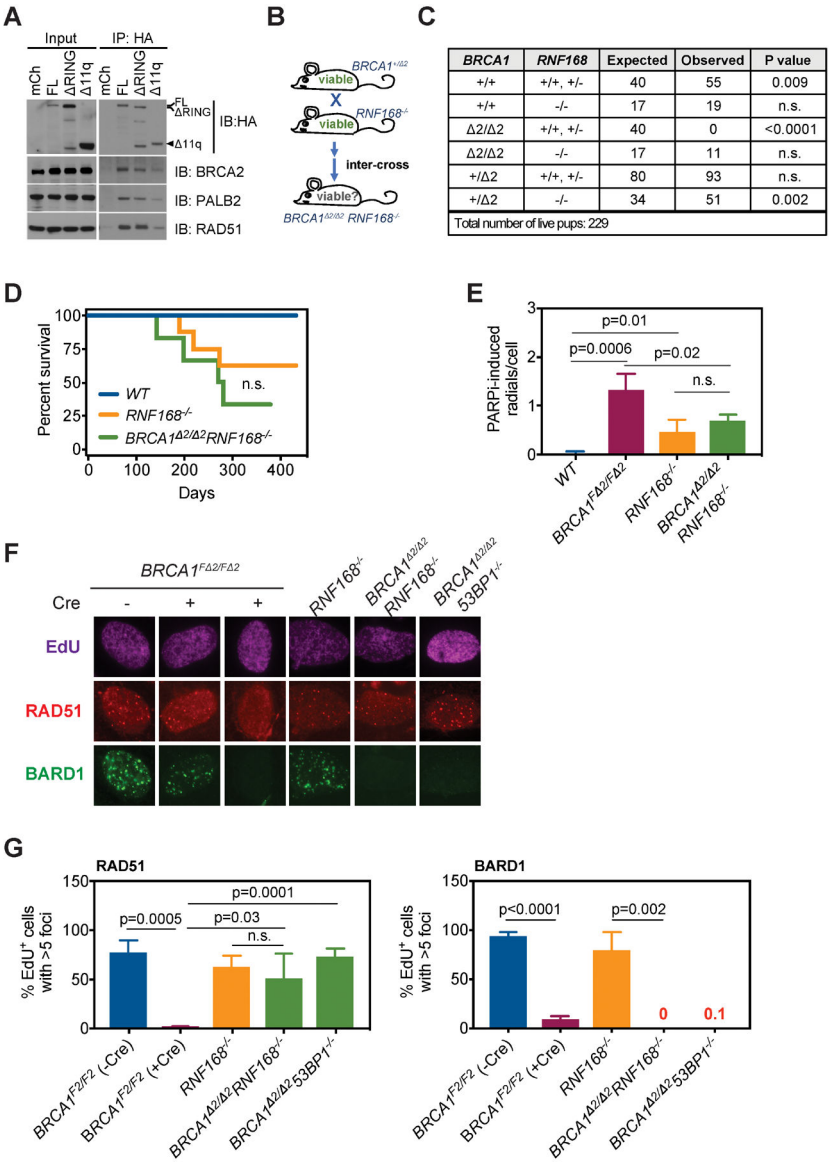

BRCA1	RNF168	Expected	Observed	P value
+/+	+/+, +/-	40	55	0.009
+/+	-/-	17	19	n.s.
Δ2/Δ2	+/+, +/-	40	0	<0.0001
Δ2/Δ2	-/-	17	11	n.s.
+/Δ2	+/+, +/-	80	93	n.s.
+/Δ2	-/-	34	51	0.002
Total number of live pups: 229				

Figure 5. RNF168 function is dispensable in a BRCA1 mutant that retain interaction with PALB2.

(A) Co-immunoprecipitation of BRCA1-interacting proteins in BRCA1-null human MDA-MB436 cells stably expressing full-length (FL), ΔRING and Δ11q isoforms of BRCA1. Cells expressing empty vector (mCherry) were used as control.

(B) Breeding strategy for the generation of mice lacking *RNF168* in the context of homozygous *BRCA1*$^{\Delta 2/\Delta 2}$ mutation.

(C) Summary of breeding outcomes from two intercrosses: *BRCA1*$^{+/\Delta 2}$*RNF168*$^{+/-}$ X *BRCA1*$^{+/\Delta 2}$*RNF168*$^{+/-}$ and *BRCA1*$^{+/\Delta 2}$*RNF168*$^{+/-}$ X *BRCA1*$^{+/\Delta 2}$*RNF168*$^{-/-}$.

(D) Kaplan-Meier survival analysis of *WT* (n=6), *RNF168*$^{-/-}$ (n=9) and *BRCA1* $^{\Delta 2/\Delta 2}$*RNF168*$^{-/-}$ (n=6) mice. Overall survival was comparable between *BRCA1* $^{\Delta 2/\Delta 2}$*RNF168*$^{-/-}$ and *RNF168*$^{-/-}$ mice (p=0.31).

(E) The average number of chromosomal radials per metaphase spread in *WT*, *BRCA1*$^{F\Delta2/F\Delta2;\ CD19Cre}$, *RNF168*$^{-/-}$ and *BRCA1*$^{\Delta2/\Delta2}$ *RNF168*$^{-/-}$ B cells exposed to PARPi.

(F) RAD51 and BARD1 foci formation in *WT* (*BRCA1*$^{F\Delta2/F\Delta2}$ no Cre), *BRCA1*$^{\Delta2/\Delta2}$ (*BRCA1*$^{F\Delta2/F\Delta2}$+Ad-Cre), *RNF168*$^{-/-}$ and *BRCA1*$^{\Delta2/\Delta2}$ *RNF168*$^{-/-}$ MEFs 4 hours post γ-irradiation (5 Gy). Note that a small fraction (<10%) of *BRCA1*$^{F\Delta2/F\Delta2}$+AdCre MEFs retain robust BARD1 foci formation under these conditions. The majority of such cells also stain positive for RAD51 foci.

(G). The percentage of EdU-positive (S-phase) *WT* (*BRCA1*$^{F\Delta2/F\Delta2}$ no Cre), *BRCA1*$^{\Delta2/\Delta2}$ (*BRCA1*$^{F\Delta2/F\Delta2}$+Ad-Cre), *RNF168*$^{-/-}$ and *BRCA1*$^{\Delta2/\Delta2}$ *RNF168*$^{-/-}$ MEFs that stained positive for RAD51 (left panel) or BARD1 (right panel) foci 4 hours post γ-irradiation (5 Gy). For *BRCA1*$^{F\Delta2/F\Delta2}$+AdCre MEFs, RAD51 foci formation was assessed in BARD1-negative cells.

Data in E and G are presented as mean ± SD. In C, D and E/G, statistical significance was calculated using χ^2 test for goodness of fit, Mantel-Cox test and unpaired two-tailed Student's *t*-test, respectively.

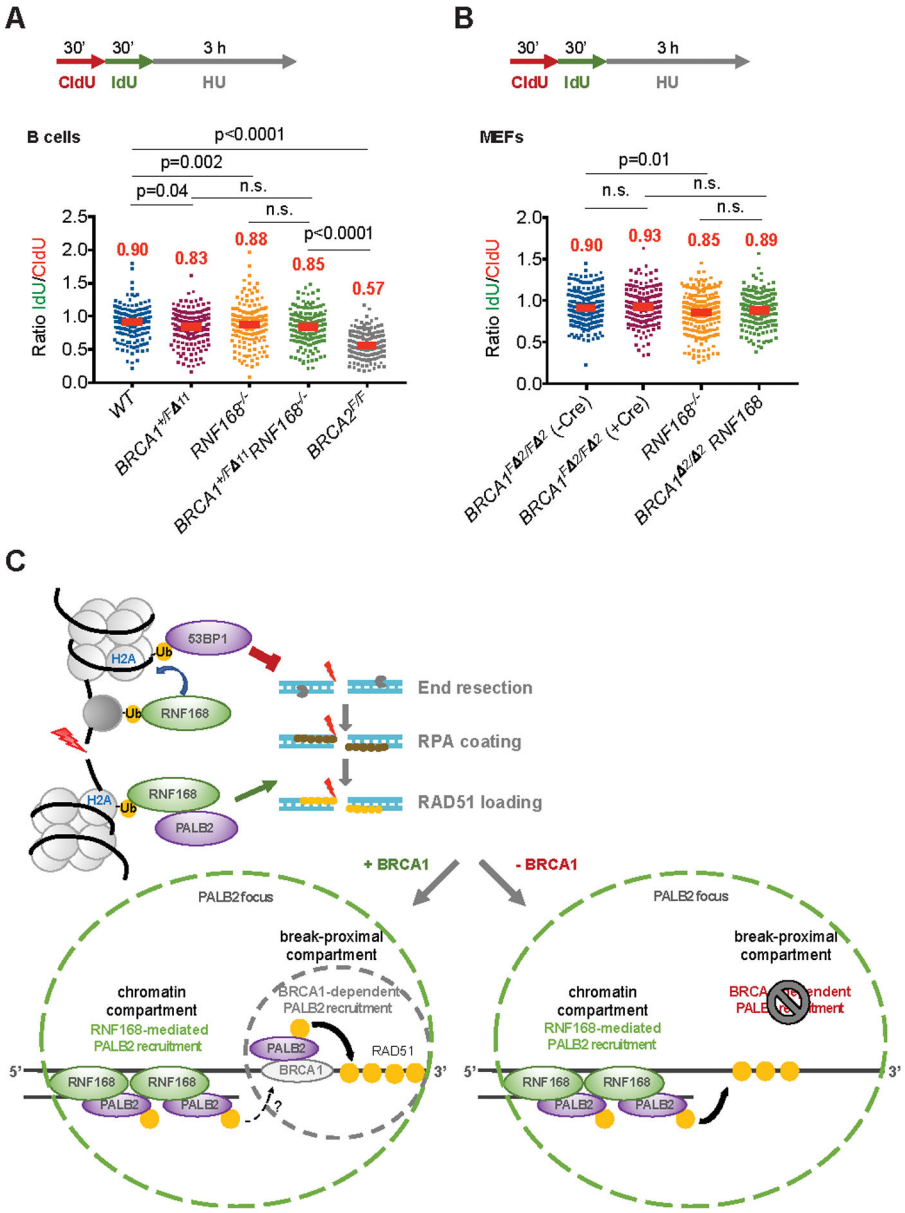

Figure 6. RNF168 does not cooperate with BRCA1 in the protection of stalled replication forks.

(A) Ratio of IdU vs. CldU incorporation in *WT*, *BRCA1*$^{+/FΔ11;\ CD19Cre}$, *RNF168*$^{-/-}$ and *BRCA1*$^{+/FΔ11;\ CD19Cre}$ *RNF168*$^{-/-}$ B cells following hydroxyurea (HU) treatment. *BRCA2*$^{F/F;\ CD19Cre}$ B cells were used as a positive control for HU-induced nucleolytic degradation of nascently replicated DNA. Schematic for labeling B cells with CldU and IdU is shown at the top.

(B) Ratio of IdU vs. CldU incorporation in *WT* (*BRCA1*$^{FΔ2/FΔ2}$ no Cre), *BRCA1*$^{Δ2/Δ2}$ (*BRCA1*$^{FΔ2/FΔ2}$+Ad-Cre), *RNF168*$^{-/-}$ and *BRCA1*$^{Δ2/Δ2}$ *RNF168*$^{-/-}$ MEFs following HU treatment. Schematic for labeling MEFs with CldU and IdU is shown at the top. Data shown in A and B are compiled from two independent experiments. Statistical significance was calculated using the Mann-Whitney test.

(C) A working model depicting how RNF168 cooperates with BRCA1 during HR. RNF168 regulates HR at two distinct steps. First, RNF168 recruits 53BP1 to limit end resection. Once nucleolytic processing of the break is underway, RNF168 additionally recruits PALB2 to the ssDNA compartment or chromatin flanking the break site. In BRCA1-proficient cells, loading of RAD51 is likely to be primarily carried out by the BRCA1/PALB2/BRCA2 complex that accumulates on the processed ssDNA, while RNF168/PALB2 may also assist in RAD51 assembly. As a result, loss of RNF168 in BRCA1-proficient cells produces only relatively subtle HR defects. However, if the canonical BRCA1/PALB2/BRCA2 pathway is absent or limiting in its functionality, RNF168-mediated PALB2 recruitment to ssDNA or chromatin provides an essential alternative route for RAD51 loading. Abrogation of RNF168 activity in BRCA1 compromised cells results in dramatically elevated genome instability, which may promote tumorigenesis.